



VICTORIA UNIVERSITY
MELBOURNE AUSTRALIA

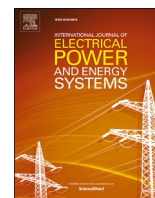
Fire probability risk ranking of vegetation species in vegetation high impedance faults

This is the Published version of the following publication

Ozansoy, Cagil and Sianaki, Omid (2024) Fire probability risk ranking of vegetation species in vegetation high impedance faults. *International Journal of Electrical Power and Energy Systems*, 157. ISSN 0142-0615

The publisher's official version can be found at
<https://www.sciencedirect.com/science/article/pii/S0142061524000255?via%3Dihub>
Note that access to this version may require subscription.

Downloaded from VU Research Repository <https://vuir.vu.edu.au/48395/>



Fire probability risk ranking of vegetation species in vegetation high impedance faults

Cagil Ozansoy^{a,*}, Omid Ameri Sianaki^b

^a College of Sport, Health, and Engineering, Victoria University, Melbourne, Australia

^b College of Arts, Business, Law, and IT, Victoria University, Melbourne, Australia

ARTICLE INFO

Keywords:

Vegetation species
Fire-risk
Vegetation to conductor contacts
High impedance faults

ABSTRACT

This work presents an analytical approach into fire-risk ranking of vegetation species during VeHIFs. One prior approach to such a fire risk assessment involved the consideration of the amount, size, and temperature of embers falling from branches. This work proposes a purely analytical methodology based on the analysis of average/maximum magnitudes of odd-harmonics current signatures released from species during VeHIF events. This analytical approach relates to the premise that emission of fault signatures is dependent on the ignition stages that a species experiences, while subject to a conductor-to-tree contacts. High-risk species experience volatile fault currents, with volatility being a sign of physical charring, subsequently leading to heightened ember formation. This volatility in the fault currents of high-risk species also results in higher levels of odd-harmonic current signatures. The temporal growth rate of odd-harmonics is the second critical factor, with elevated fire-risk observed in slow temporal fault current growth species. This is linked to the fact that when the fault current growth is slow, this elevates the fire-risk in terms of increased times for traditional over-current methods to clear the fault. *Salix* and *S. Molle* have been determined as the highest and lowest risk species respectively. Findings are compatible with observatory analysis on ember formation.

1. Introduction

Vegetation High Impedance Faults (VeHIFs) have impacted us through bush fire starts in many ways including loss of lives, physical injuries and psychological distress. Most academic research is heavily steered towards developing techniques to detect or localise faults. Significant knowledge gaps exist in the selective conductivity and fire-risk assessment of vegetation species. Vegetation management is a major operational cost for the power distribution industry. Effective vegetation management strategies are critical in refining adopted practices to balance risk and cost providing customers a balance of safety and affordability. This requires an increased awareness of species with high 'fire-risk' probability and high 'un-classification' risk probability. This could lead to maximum clearance standards for various species in minimizing the risk of fire starts or undetected phase-to-e (ph-to-e) faults in bushfire hazard areas. It also necessitates a better awareness of species with a 'low fire probability' for their reduced clearance in better managing the health/appearance of trees in our urban and regional communities. While some species may be categorized as 'low fire probability', earth faults occurring through such species must still be detected and

appropriately cleared. This paper fills these knowledge gaps by developing a scientific and analytical method of analysing species in terms of their low-order odd harmonic current signature emissions (during faults). Novel contributions include ranking of species in terms of their VeHIF induced odd-harmonic current signature magnitudes as well as the speed of temporal growth of these signatures. This research work seeks to link the 'fire-risk' probability rankings of the species to their odd-harmonic current signature emissions and temporal growth of these signatures.

2. Fire probability categorization of species

During the 'Vegetation Conduction Ignition Testing' project [1], vegetation species were classified through staged vegetation HIF tests. Table 1 shows the average fire probability ranking of species as given in [2]. In [2], risk categorisation began with an assessment of whether a particular test was a 'fire producing' or 'not a fire producing' test. This was based on the amount/size/temperature of embers that fell from the species, during the test, on to the test-rig floor. A 'branch on wire' (phase-to-earth) test was taken as a fire producing test if the following

* Corresponding author at: College of Engineering and Science, Victoria University, Melbourne, Australia.

E-mail address: cagil.ozansoy@vu.edu.au (C. Ozansoy).

<https://doi.org/10.1016/j.ijepes.2024.109804>

Received 3 August 2023; Received in revised form 26 November 2023; Accepted 16 January 2024

Available online 23 January 2024

0142-0615/Crown Copyright © 2024 Published by Elsevier Ltd.

This is an open access article under the CC BY-NC-ND license

(<http://creativecommons.org/licenses/by-nc-nd/4.0/>).

Table 1
Fire Probability Risk Categorization of Vegetation Species [2].

Species	Average Fire Probability
Salix (Willow)	1
Fraxinus Angustifolia (Desert Ash)	0.58
Acacia Mearnsii (Black Wattle)	0.57
Pinus Radiata (Radiata Pine)	0.55
Eucalyptus Baxteri (Stringybark)	0.53
Eucalyptus Viminalis (Manna Gum)	0.50
Acacia Melanoxydon (Blackwood)	0.23
Cotoneaster Glaucophyllus (Cotoneaster)	0.21
Acacia Pycnantha (Golden Wattle)	0.10
Pittosporum Undulatum (Native Daphne)	0.07
Allocasuarina Verticillata (Drooping Sheoak)	0.05
Schinus Molle (Peppercorn)	0.00

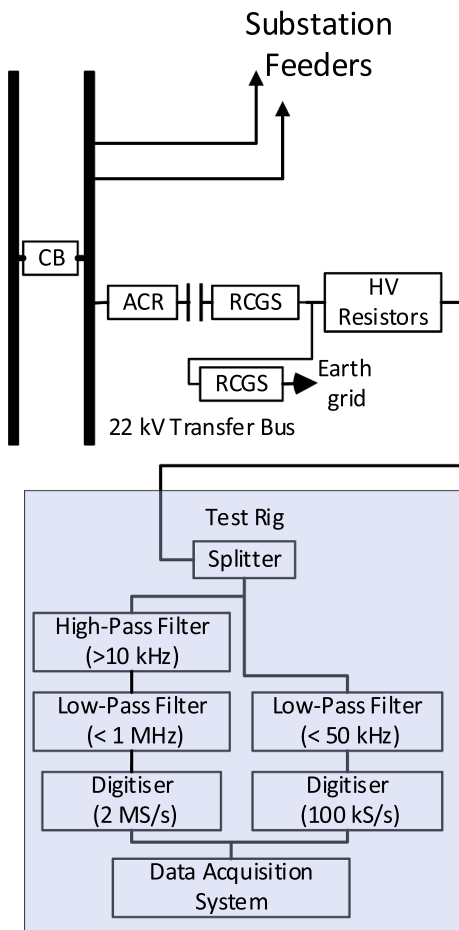


Fig. 1. Test rig and measurement system.

conditions were met [2]:

- “Embers fell to the floor of the test rig and remained glowing for at least a second” [2]; and
- “If the embers were small, e.g. small leaves, ember temperature exceeded 350 °C” [2]; or
- “If embers were large, e.g. burned twig, ember temperature exceeded 250 °C” [2].

As shown in Table 1, Salix was given the highest fire probability in [2]. The average fire probability for each species was given through statistical analysis of 1-A limit fault tests. For example, out of the fourteen 1-A limit phase-to-earth (ph-to-e) fault tests of the species Acacia Mearnsii, only eight satisfied the conditions given above, therefore

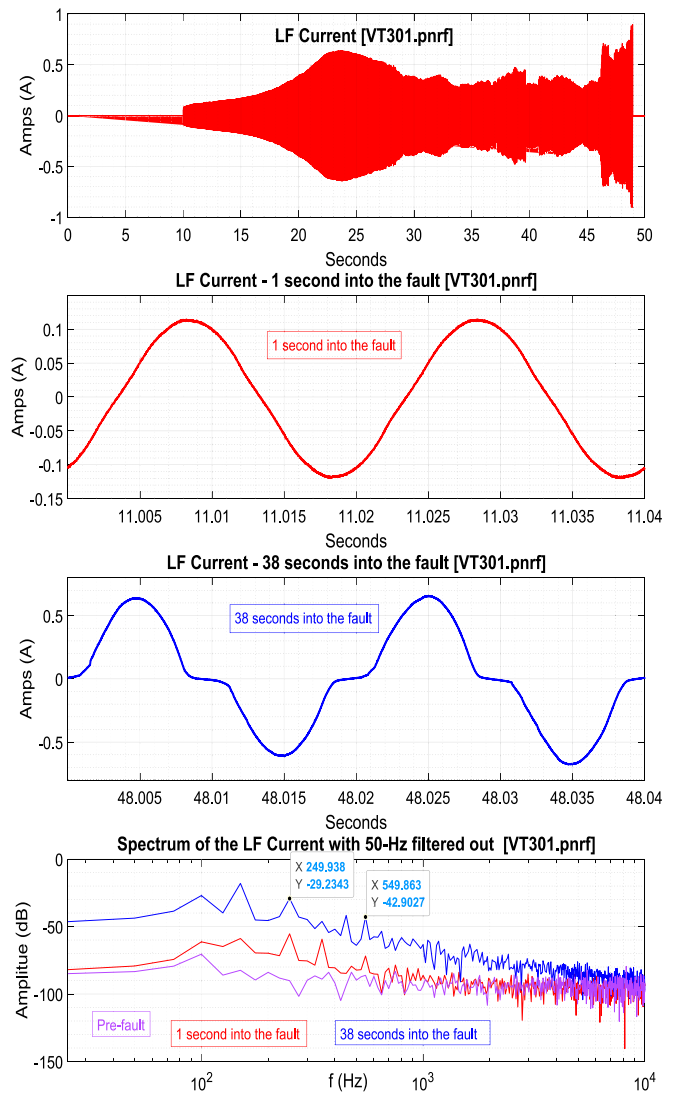


Fig. 2. First row: LF current during a VEHIF. Second row: I_f at the 11 s (1 s into the fault). Third row: I_f at the 48 s (38 s into the fault). Fourth row: Spectral comparison of the harmonics at 11 s and 48 s with 50-Hz filtered.

equating to an average probability of ~57 %. For Pittosporum Undulatum, only one out of the fifteen valid tests was observed to meet the amount/size/temperature condition of the embers for a total average risk probability of ~7 %.

3. Literature review

Other literary research exists on understanding the vegetation conductivity of tree-to-conductor contacts. While works in HIF detection/localization are abundant, that is not the case for the species electrical conductivity and fire-risk comparison. In 2007, one EPRI project [3] investigated touch potential risks in tree-to-conductor contacts. The project studied voltage gradients and fault currents created, when distribution conductors came into physical contact with trees. The focus in [3] was on ‘characterizing electric touch potential voltages and current levels to which a person on the ground would be exposed’ instead of a comparative assessment of the fire-risk levels of species [3]. Limited results were still presented in [3], that shed light on two species: the Pin Oak (Q. Palustris) and Silver Maple (A. Saccharinum). In single contacts, the measured voltage (at a height of 1.5 m) was slightly higher for the Maple, whereas the fault current (I_f) through Oak was higher. A third species, the Austrian Pine (P. Nigra), was also tested in a follow-up

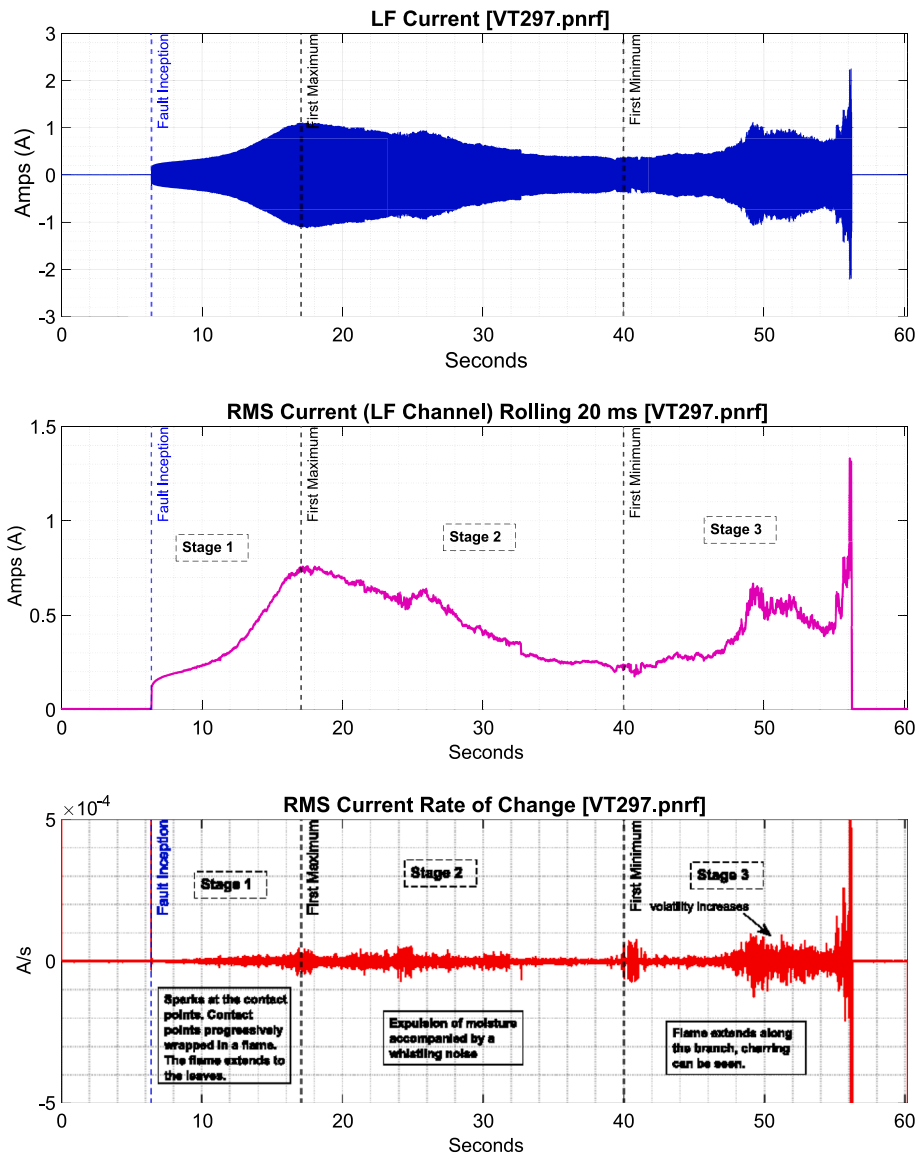


Fig. 3. Fault current (I_f) development in the high fire risk species of *Salix Sp.* First row: the sampled I_f . Second-row: I_{f-rms} . Third-row: dI_{f-rms}/dt . (VT297).

project [4] in 2008. The focus was still on measuring I_f levels and voltage gradients along the fault pathway from point of contact to earth. In terms of the average maximum I_f (averaged using three test results in [4]), the species ranked high to low as the Oak (96 mA), Pine (69 mA), and Maple (24 mA).

Characterization of the physical/electrical phenomena related to vegetation contacts on distribution conductors was previously presented in [5]. In [5], authors suggest that progressive charring (carbonization) is key to establishing a low-current path and they also state that fault current increases in a non-uniform manner as charring increases. The transition from a fault current (I_f) of few amperes to a high-current condition was argued to occur very suddenly when the carbonized path is complete [5]. Further HIF experimental tests were given in [6] on detecting a specific case of HIF caused by white stork nests. They were argued to produce faults similar to trees, when parts of the nest cause electrical contact between the conductor and the earthed steel tower. In [7], the authors discussed staged fault testing for HIF data collection on a range of surfaces including concrete, gravel, asphalt, and a tree. In the conducted freshly cut Pine tree experiment, the tree was observed to sustain the fault for 13 min without blowing the fuse, after which the test was concluded [7]. Hou discussed staged HIF tests in [8] where the voltage and current signals were recorded both at the substation and test

site on ground surfaces including concrete blocks, grassy earth, asphalt and tree limbs. Just like many other works in the field [9–12] which either focus on HIF detection or localisation, the discussion in [8] also revolved around a new HIF algorithm with an IIR limiting average and adaptive tuning. As shown from this sift of literary works, research into comparative risk-evaluation of species is indeed scarce.

Vegetation High Impedance Faults (VeHIFs) detection using low order odd-harmonic indicators have frequently been proposed in the literature [13]. These often include statistical, frequency-domain, fuzzy logic and Artificial Intelligence (AI) based analysis of magnitudes and phase angles of harmonic combinations such as the third, fifth, and second harmonics [14,15]. The study [16] by Jeerings and Linders, focusing on the phase angle relationship between the current's third-harmonic and the voltage reference, was pioneering in leading the path for preceding works. Wang et al. cautioned in [17] that the orders, magnitudes and phase angles of harmonics may be different under different HIF parameters [17].

4. Research aims and originality

This work performs fire-probability risk assessment of species using an analytical bases by examining fault currents recorded for the various

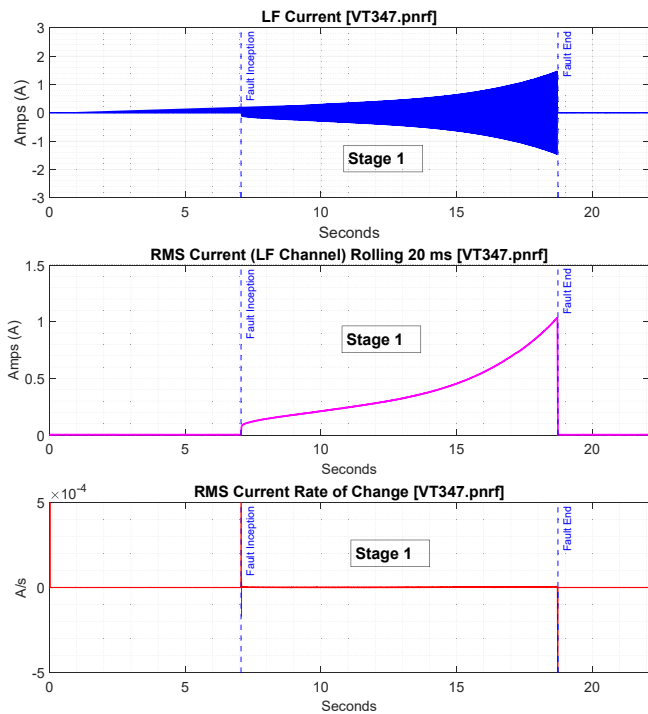


Fig. 4. Fault current (I_f) development in the low fire risk species of *S. Molle*. First-row: the sampled I_f . Second-row: I_{f-rms} . Third-row: dI_{f-rms}/dt . (VT347).

species. It aims to fill the knowledge gap in regards to comparison of species in terms of their Low-Frequency (LF) odd-harmonic emissions. A key contribution is the analysis of harmonic based indicators, their magnitudes, and rate of growth in various species during VeHIFs. Marxsen argues in [2] that detecting earth faults in two seconds of the fault current reaching 0.5-A can result in a tenfold fire-risk reduction. Hence, it is not sufficient to detect VeHIF faults, but to clear them quickly to minimize the fire-risk. This work also sheds light on the potential speed of detection possible (through temporal growth comparison of odd-harmonics) in several species. A dataset of 156 ph-to-e ‘branch touching wire’ $1-A_{rms}$ limit VeHIF faults will be used in this scientific analysis. In [2], the rules were applied by reviewing infrared videos produced by a thermal camera, which had the capability to locate the hottest points in the images and show their temperatures in the top-left corner of the screen. While not explicitly stated in [2], the review of the infrared videos appears to have been a manual process and un-automated (i.e. no AI-based image processing was used). The analysis herein differs from [2] in that authors use a scientific method of analysing species in terms of emissions of low-order odd harmonic current signatures from these species. Our findings will be compared to the species rankings in [2] to contrast outcomes to the ember formation based methodology in [2]. Target harmonic signatures include the third (hrm_3), fifth (hrm_5), seventh (hrm_7), ninth (hrm_9), eleventh (hrm_{11}), thirteenth (hrm_{13}), and fifteenth harmonics. In referring to all odd-harmonics, we will use the nomenclature hrm_{all} . This work addresses the following research questions:

- (i) What are the differences in the odd harmonic current signatures of high fire-risk and low fire-risk species?
- (ii) Can we develop a risk score of species by solely examining their odd-harmonic current signatures? Would such an analysis be compatible with that given in [2]?
- (iii) Is there a link between conductivity of a species and the amount of odd harmonic current signatures it generates? What about a link between ember formation during the ignition of a species and the odd-harmonic current signatures it generates?

- (iv) On which species would the odd-harmonic signatures grow the fastest and slowest? On which species would faults be harder to detect using non-traditional Over-Current (OC) based methods?
- (v) Is there a link between the ‘fire-risk’ ranking of a species and its ‘un-classification’ risk using novel methods?

At the core of our scientific methodology lies the analysis of the frequency-domain Fast Fourier Transform (FFT) magnitudes of the first seven odd-harmonic current signatures (VeHIF induced) using 20-ms sweeps repeating the computation once a second. The FFT data will later be analysed, averaged, or cumulatively summed to develop metrics and to reach certain conclusions on the research questions raised above. The same will be used for the temporal growth speed analysis with each sweep equating to a second. The work herein differs from other comparable works in that low order odd-harmonic indicators will be used for the electrical conductivity and fire-risk analysis of species, rather than in proposing a new protection method. This work does not propose a VeHIF detection method, but primarily an analytical evaluation of vegetation species fire-probability risk ratings. Implementation of an odd-harmonics based HIF detection scheme is outside the scope of this work.

5. Methodology and ignition stage analysis

The validation dataset is from staged VeHIF tests performed for the ‘Vegetation Conduction Ignition Testing’ project in 2015 [2]. The project focused on sampling and testing of diverse vegetation species in staged HIFs in a test rig (see Fig. 1). Phase-to-earth (ph-to-e) fault tests involved a tree branch laid across two conductors, one energized with the 12.7 kV phase voltage and the other earthed. The Low Frequency (LF) channel (DC to 50 kHz) sampled the fault current continuously with a 100 kSa/s sampling rate. In all analyzed tests, the pre-set fault current threshold varied from 0.5 Amps to 4 Amps (through the use of a current limiting resistor). Each experiment was terminated by removing the HV supply to the energized conductor, once the threshold value was reached. The primary voltage transducer was a 1.1-nF rated 24-kV working voltage Coupling Capacitor (CC). Using one 11-m coaxial cable, the CC was connected to a Capacitive Voltage Divider (CVD) with a voltage ratio of 2000:1 at 50 Hz.

The LF current was recorded with the test terminated upon the fault current (I_f) reaching the set current limit: $1 A_{rms}$ as in the example of Fig. 2 for the test labelled as VT301. Comparing the I_f plot at the 11 s (1 s into the fault relative to the fault start time at 10 s) with the 48 s (38 s into the fault) plot in Fig. 2, a significant uplift in the LF spectrum can be observed (including major growth in harmonics) when arcing is more aggressive in the 48 s.

Fig. 3 shows the LF recording during a ph-to-e VeHIF test (*Salix Sp.*) labelled as VT297. The test was terminated after I_f reached $1 A_{rms}$. Various stages of ignition development [2] can be identified for VeHIFs. These stages are the contact development (Stage 1), moisture expulsion (Stage 2), and progressive charring (Stage 3) [2]. As in Fig. 3, Stage 1 is dominated by a progressive increase in the plasma until I_f reaches its first maximum. In Stage 2, I_f falls due to the expulsion of the moisture which dries out the species leading to its resistance to increase. Finally, in Stage 3, charring begins accompanied by breakout of flames. During charring (see Fig. 3), arcs appear in the flame causing I_f volatility. I_f volatility (a sign of charring) peaks around the first local minimum (after the first maximum) [18]. One key conclusion in [2] was that when a species undergoes a high degree of charring, ignition at height is more likely to result in embers with the size and temperature conditions for fire ignition at ground level. Fig. 4 shows a Stage 1 only fault (VT347) for the low fire risk species of *Schinus Molle*.

During VT347 (see Fig. 4), sparks were formed at the contact points, but flames did not break out and there was little ember formation. It is likely that I_f would have grown larger in a real life setting and finally detected by overcurrent protection elements. The test was interrupted after 12 s, as I_f reached the set threshold. Fig. 5 shows another Stage-1

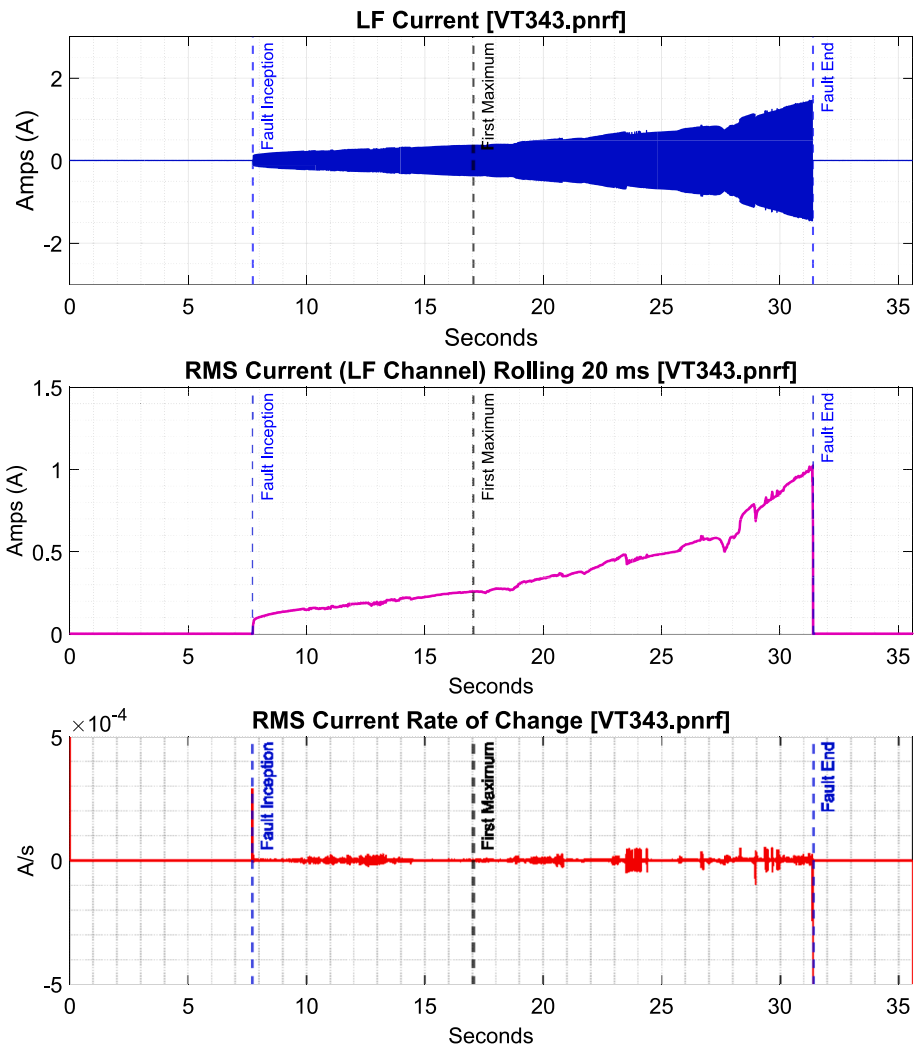


Fig. 5. Fault current development in the low fire risk species of *S. Molle*. First-row: the sampled I_f . Second-row: I_{f-rms} . Third-row: dI_{f-rms}/dt . (VT343).



Fig. 6. Physical state of the branch during a fault of the low fire risk species of *S. Molle* (VT343). Charring is seen at/nearby the contact points. The charring does not get sustained as breakout of flames and the branch does not catch fire. Embers are formed and released, but these extinguish almost instantaneously upon hitting the ground. Image from [1].

only I_f development during VT343, a test of the same low risk species of *S. Molle*. As in Fig. 5, I_f is slightly more volatile, but still increases rapidly. Fig. 6 shows the physical ignition state of the branch during the test. The sparks were formed at/nearby contact points, but they failed to turn into flames and the branch did not really catch fire. More embers were released from the branch in VT343 (as compared to VT347), but these extinguished almost instantly upon hitting the ground. A key

characteristic separating high bushfire risk species from a low risk species is therefore the stages of ignition that it goes through. In the specific example of Fig. 6, the shown branch is not very leafy. During the project [1], close to one thousand tests were performed using vegetation samples of various moisture, conductivity, branch diameter/size, and leafiness conditions [2]. In this work, authors use 156 of these tests capturing a broad spectrum of influencing factors such that research findings can be generalized.

6. Voltage–current characteristic comparison of species as per the fire probability risk

Intermittent arcs of varying widths often escort VeHIF currents [19]. In [20], a method was presented for identifying the I_f arcing level. This method was further adapted herein for estimating the number of samples in each 20 ms window recording where I_f will be in its $-0.02 \times |I_{f-max}| < I_f < 0.02 \times |I_{f-max}|$ range. The objective is to show the correlation between arcing and fire-probability risk. Fig. 7 contrasts the time-based arching levels in four tests using the lowest risk (*S. Molle*) and highest risk (*Salix*) species. As in Fig. 7, tests of the highest-risk species of *Salix* experience much higher levels of arching, when compared to those of the *S. Molle*. Fig. 8 shows the arching level in I_f at various 20-ms window time spaced intervals (signposted on the top LF current graph) during VT297. All waveforms are in p. u. using the base values of 2.27 A and 17.3 kV. As in Fig. 8, arcing is intermittent with fluctuating levels due to conduction

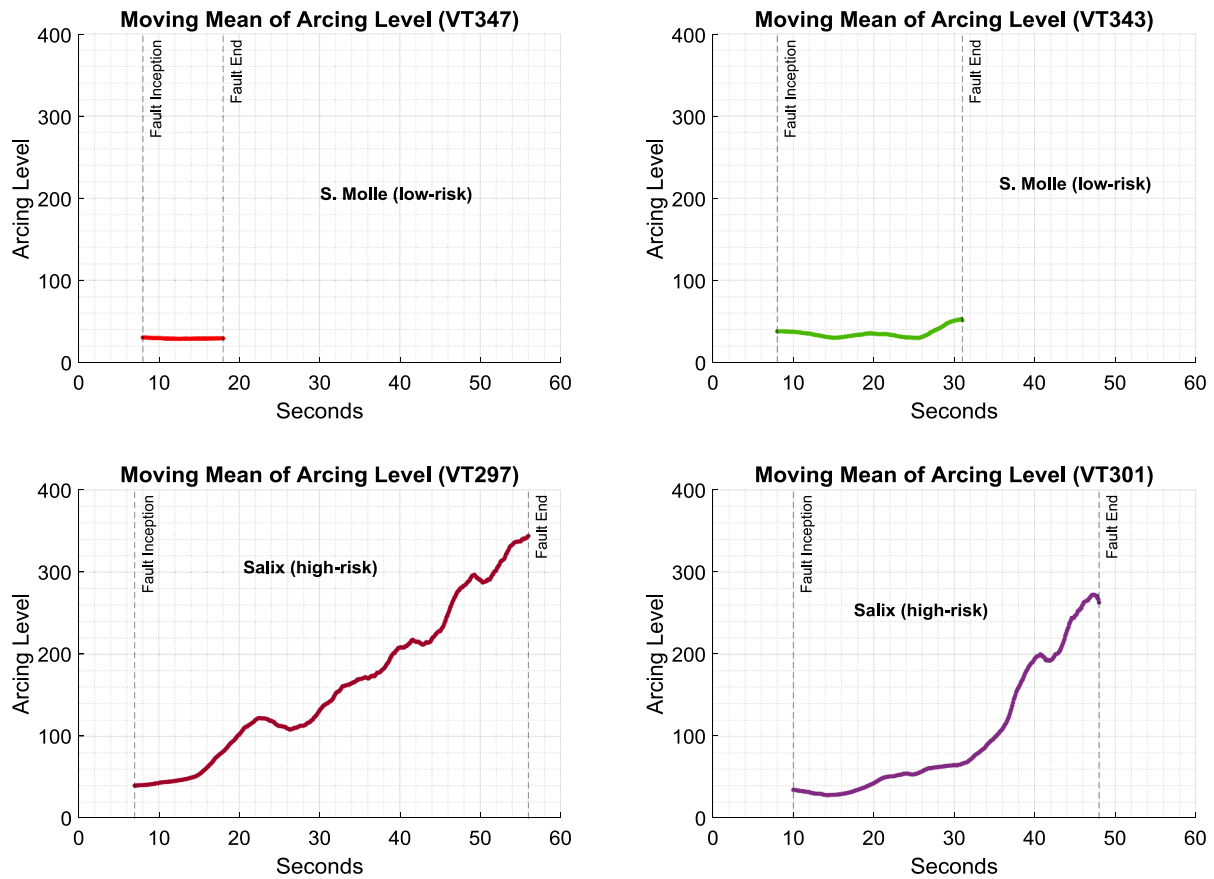


Fig. 7. Temporal arcing variation in the fault currents of four tests.

through a non-linear impedance. When arcing occurs, it extinguishes near the zero-crossings due to inadequate voltage levels for sustaining the discharge. It reignites once voltage recovers to a level where the discharge can be sustained again. Fig. 8 also highlights the changes occurring in the voltage-current (V-I) characteristic of the VeHIF fault current as arcing increases from fault start to end. At 8 s, when the arcing level is low, there is almost a linear relationship between the fault current and voltage. As fault progresses with an increase in arcing, the V-I relationship starts to resemble a skewed figure-eight with widening loops. This is in line with results previously reported in the literature particularly with the V-I characteristic in [21], while this gradual shift in the V-I characteristic (due to increasing arcing) from an almost linear line to the skewed elliptic figure-eight pattern is being first reported here in this transparency. Fig. 9 compares the V-I characteristic of four tests of two species using their over-fault sampled voltage and current datasets.

In the academic literature, researchers [14,21–23] have reported similar V-I characteristics under different HIF contact medium conditions and settings (lab/field tests), but none have previously explicitly validated the impact of arcing level on V-I characteristic. As in Fig. 9, the skewed figure-eight loops are visually visible for the tests associated with the high-risk Salix species, whereas skewed triangular shaped V-I characteristic was formed (by the full test duration dataset) in the case of the low-risk S. Molle species. This is yet another key contribution to knowledge herein as the impact of the species type, as the contact medium, on the arcing level and linked V-I characteristic is first being reported herein in this clarity.

7. Contrast of high & low bushfire risk species

This section compares the Salix and S. Molle species in terms of their

LF signatures (150 Hz–750 Hz). In doing the analysis, the running FFT magnitudes (linear scale) of odd-harmonics were determined using 20-ms window-size FFT computations repeated every second. Fig. 10 shows the analysis for VT291, a 1 A_{rms} limit test of Salix Sp. (Willow) lasting ~36 s. An interesting observation is that Harmonics 3, 5, 11, and 15 only reached their maximum signature levels when the test was concluded. For Harmonics 7, 9, and 13, the harmonic maximum occurred before the test ended, with Harmonic 13 reaching its maximum only 8 s into the fault. Fig. 11 shows the same analysis for VT343, a 1 A_{rms} limit ph-to-e test of the Schinus Molle (Peppercorn) species lasting only ~23 s. As in Fig. 11, the overall harmonic signatures are lower in magnitude during the 23 s duration S. Molle fault (as compared to Fig. 10 of Salix Sp.). They also all grew to their maxima only at the fault end. This shows that fault-signature emission depends on the species and particularly on the ignition stages a species experiences, after a conductor contact. Table 2 shows the average and max values of the harmonics during VT291 as well as their Standard Deviation (STD). As illustrated, both the signature magnitude and volatility decreases with an increasing harmonic order. The same analysis is given in Table 3 for the VT343 fault. As shown, the Harmonic magnitudes and their volatility are smaller in the case of the low-risk S. Molle. Besides the signature magnitudes being lower, all harmonic maximums were reached only at the end of the fault. This suggests that an earth fault involving the S. Molle species may be harder to detect (using harmonic signatures) given their low-magnitude and slow temporal growth.

Tables 4–6 contrast the average/max harmonic magnitudes and their STDs for both species. For Salix, the I_f limit was reached 36 s into the fault, whereas it only took 23 s for the same limit to be reached in the case of S. Molle. This supports the fact that S. Molle potentially presents a smaller fault impedance to the line better conducting the fundamental frequency. While I_f through the S. Molle is likely to grow larger faster,

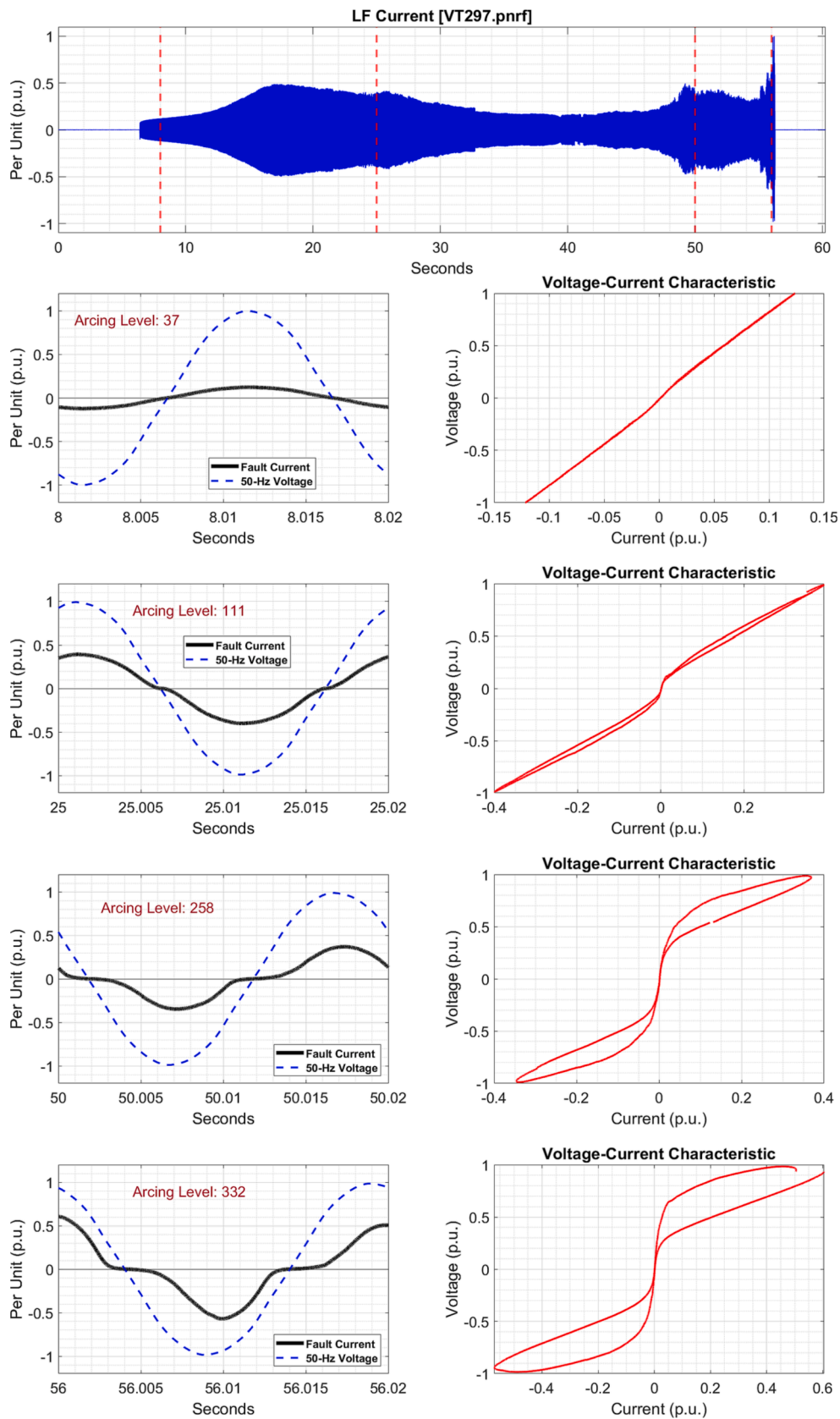


Fig. 8. Analysis of arcing levels in the fault current at various time stamps.

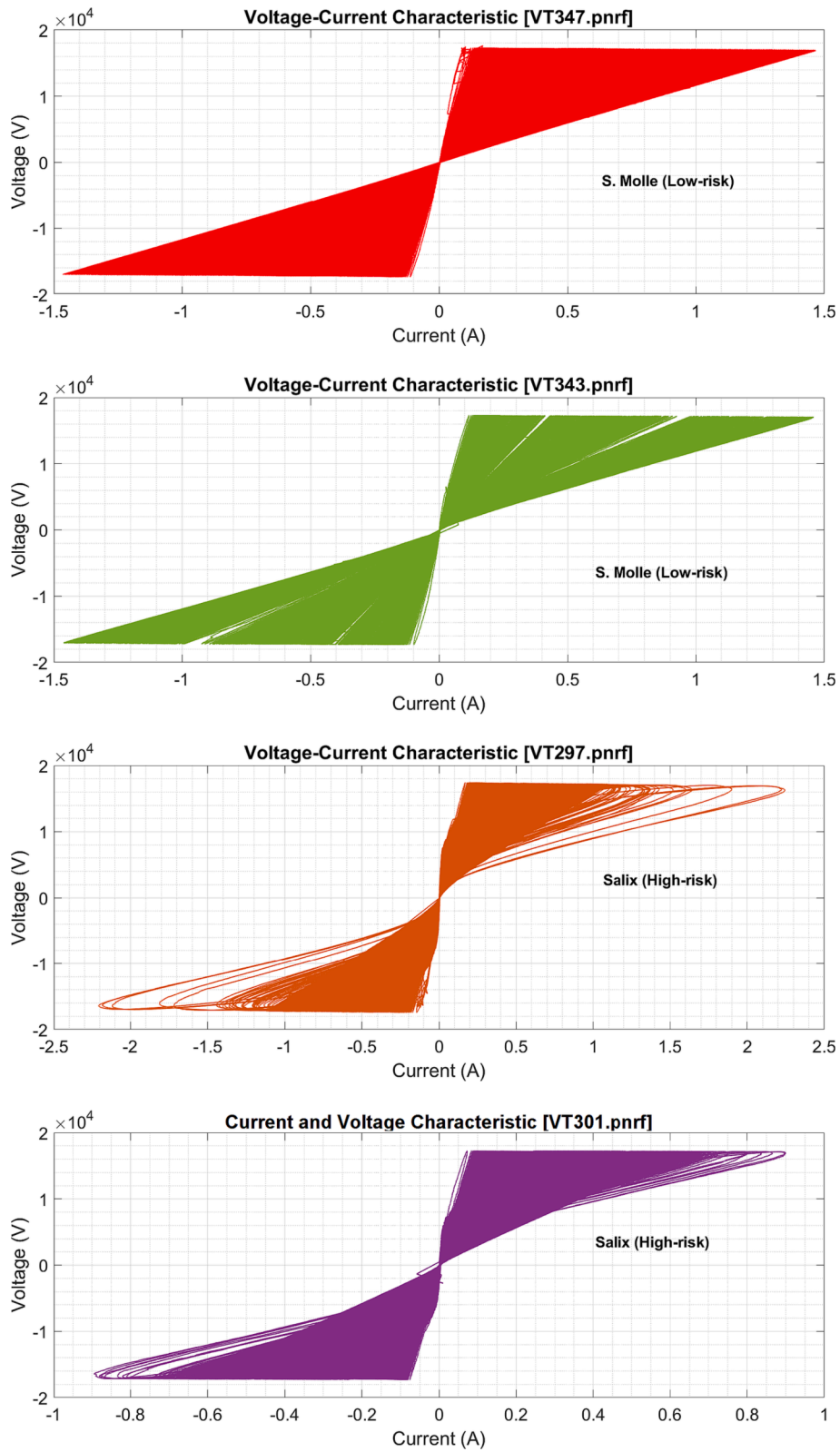


Fig. 9. Voltage-current characteristic of four fault recordings of two species.

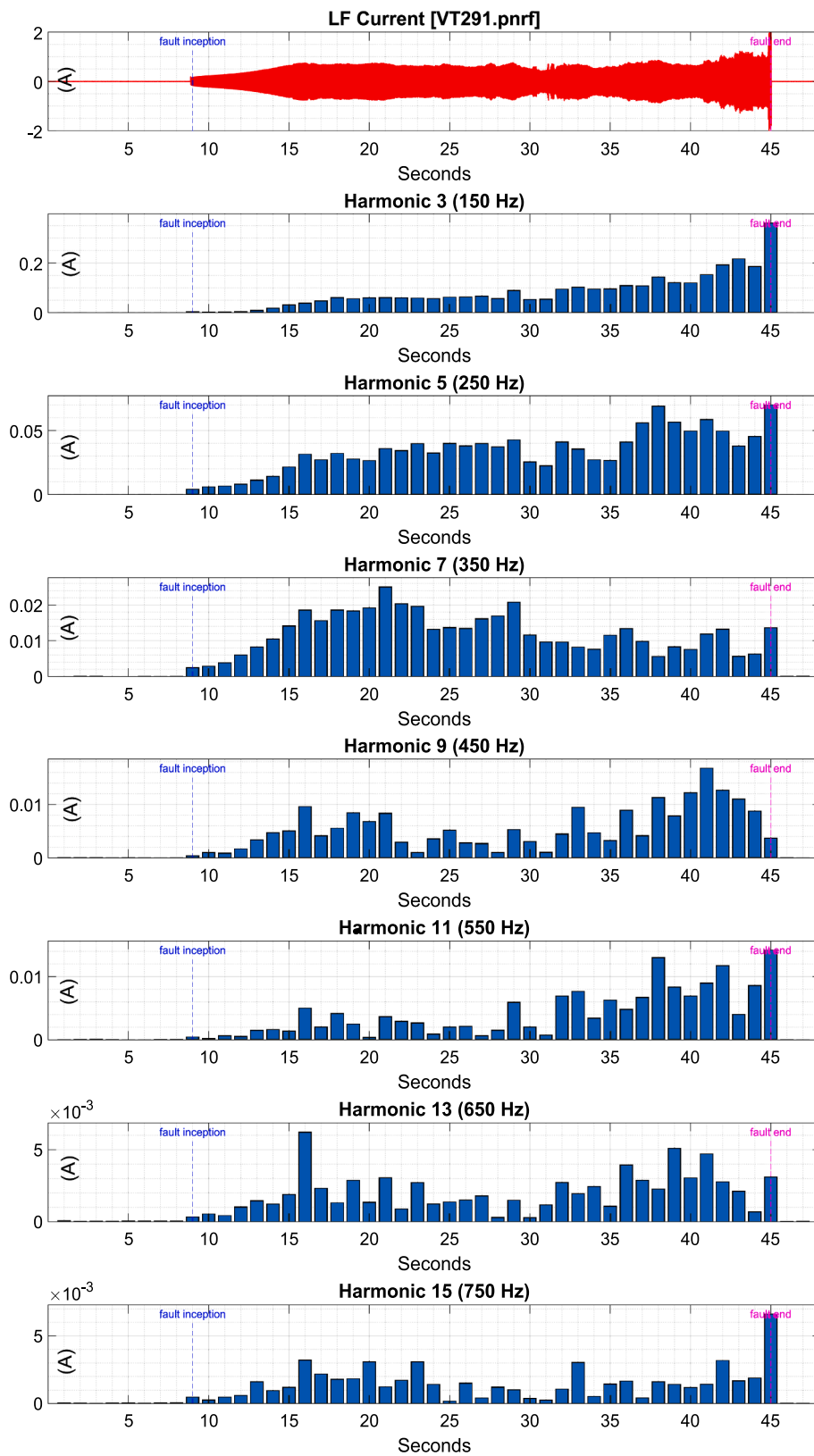


Fig. 10. LF current and odd-harmonics' FFT magnitudes. First row: I_f sampled at 100 kSa/s. Rows 2 to 7: The odd-harmonic FFT magnitudes calculated once a second using 20-ms FFT window. (VT291; Salix Sp.).

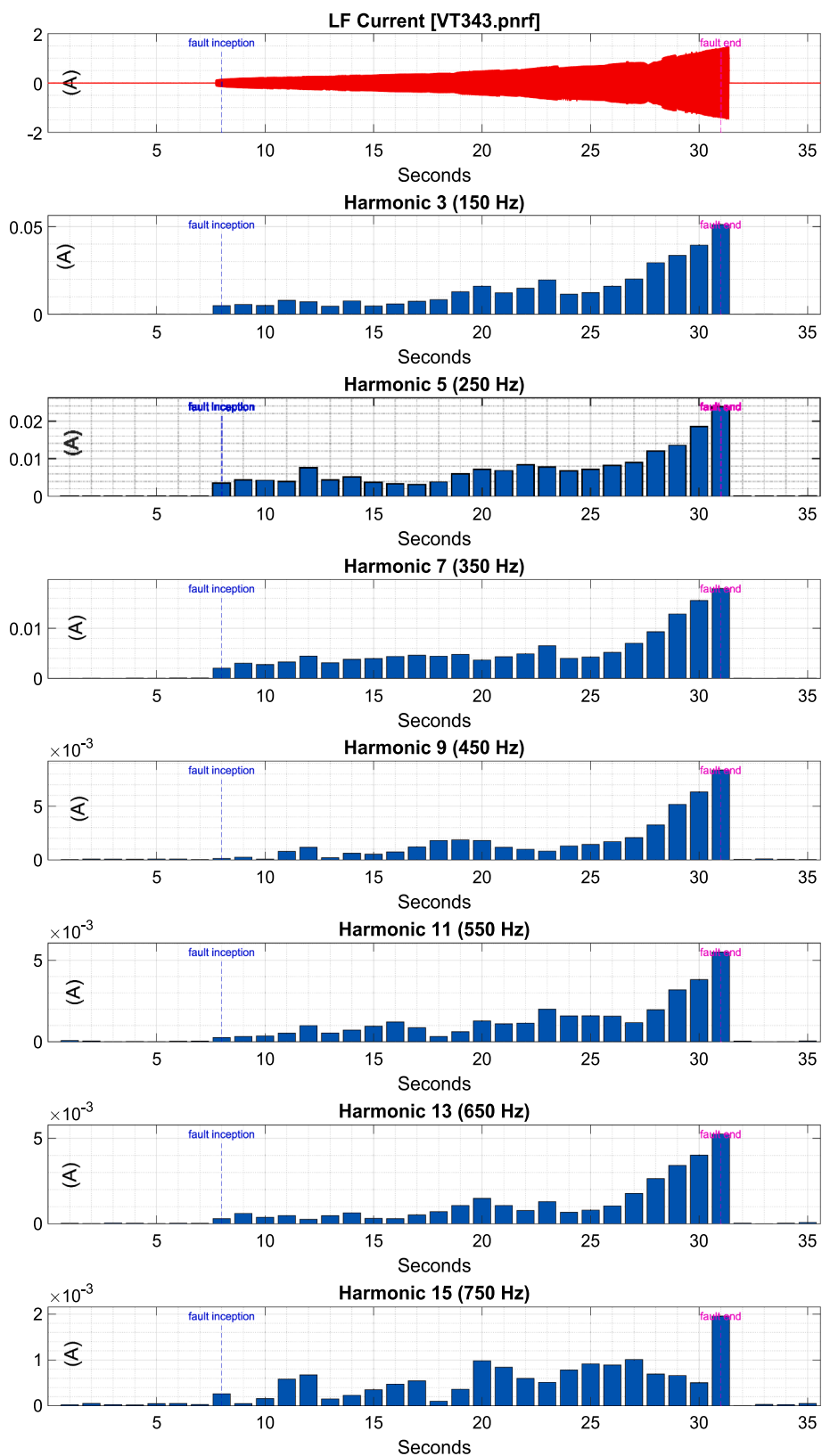


Fig. 11. I_f and odd-harmonics FFT magnitudes. First row: I_f sampled at 100 kSa/s. Rows 2 to 7: Odd-harmonic FFT magnitudes calculated once a second using a 20-ms FFT window (VT343 – S. Molle).

Table 2
Max, Average and STD of, Odd-Harmonics Currents (VT291; Salix Sp.).

f (Hz)	Max (A)	Average (A)	STD (A)
150 Hz: 3rd	0.3612	0.0847	0.0706
250 Hz: 5th	0.0701	0.0344	0.0164
350 Hz: 7th	0.0251	0.0122	0.0056
450 Hz: 9th	0.0168	0.0057	0.0039
550 Hz: 11th	0.0142	0.0043	0.0037
650 Hz: 13th	0.0062	0.0020	0.0014
750 Hz: 15th	0.0066	0.0016	0.0012

Table 3
Max, Average and STD of, Odd-Harmonics Currents (VT343; Schinus Molle).

f (Hz)	Max (A)	Average (A)	STD (A)
150 Hz: 3rd	0.0512	0.0149	0.0121
250 Hz: 5th	0.0239	0.0076	0.0050
350 Hz: 7th	0.0180	0.0058	0.0041
450 Hz: 9th	0.0084	0.0018	0.0020
550 Hz: 11th	0.0055	0.0014	0.0012
650 Hz: 13th	0.0053	0.0013	0.0013
750 Hz: 15th	0.0020	0.0006	0.0004

Table 4
Max odd-harmonic currents of the Salix Sp. and S. Molle Species.

Harmonic #	Salix Sp (Amps)	S. Molle (Amps)
Harmonic 3	0.3612	0.0512
Harmonic 5	0.0701	0.0239
Harmonic 7	0.0251	0.0180
Harmonic 9	0.0168	0.0084
Harmonic 11	0.0142	0.0055
Harmonic 13	0.0062	0.0053
Harmonic 15	0.0066	0.0020

Table 5
Average odd-harmonic currents of the Salix Sp. and S. Molle Species.

Harmonic #	Salix Sp (Amps)	S. Molle (Amps)
Harmonic 3	0.0847	0.0149
Harmonic 5	0.0344	0.0076
Harmonic 7	0.0122	0.0058
Harmonic 9	0.0057	0.0018
Harmonic 11	0.0043	0.0014
Harmonic 13	0.0020	0.0013
Harmonic 15	0.0016	0.0006

Table 6
STDs of odd-harmonic contributions of Salix Sp. and S. Molle Species.

Harmonic #	Salix Sp (Amps)	S. Molle (Amps)
Harmonic 3	0.071	0.012
Harmonic 5	0.016	0.05
Harmonic 7	0.006	0.004
Harmonic 9	0.004	0.002
Harmonic 11	0.004	0.001
Harmonic 13	0.001	0.001
Harmonic 15	0.001	0

this analysis shows that it is also the species, which is less likely to be detected through an inspection of the odd-harmonics. S. Molle was ranked as a low fire risk species due to its small amount of ember formation and the fact that forming sparks extinguished quickly. Findings in this section highlight that in species where carbonization does not take place, it is less likely to observe odd-harmonic fault signatures. A conclusion that can be drawn here is that S. Molle conducts the 50-Hz

fundamental better than Salix with less charring resulting in less harmonic signature formation. While this presents a lower fire-risk in terms of emitted embers, it makes it more challenging to detect/clear faults of the S. Molle species using odd-harmonics based methods. The fast exponential growth of I_f in the S. Molle species may result in classification by OC methods. While S. Molle was categorized as a low-risk species within the project limitations [1], it may still pose risks to the public.

As I_f was not permitted to grow beyond the set limits (in any test) [1], it is not possible to quantify how much further I_f would have grown in a low risk species such as S. Molle, or whether the branch would have finally experienced sustained charring, after being exposed to high currents over long periods. Marxsen made a point in [2] that 'species with faster I_f development tend to have lower fire-risk because the fault reaches the detection threshold of protection systems before ember production fully develops'. In line with this argument in [2], an assumption herein is that faults in such low fire-risk species would be eventually detected by traditional protection methods.

While S. Molle was categorized as a low-risk species within the project limitations [1], it may still pose risks to the public. Marxsen made a point in [2] that 'species with faster I_f development tend to have lower fire-risk because the fault reaches the detection threshold of protection systems before ember production fully develops'. In line with this argument in [2], an assumption herein is that faults in such low fire-risk species would be eventually detected by traditional protection methods.

8. Contrast of VeHIFs & other disturbances

The objective herein is to present an electrical conductivity and fire-risk analysis of species using odd-harmonic indicators. While authors do not propose a VeHIF detection method (within the scope of this paper) on the basis of odd-harmonic indicators, it is still critical to understand the efficacy of harmonic indicators in truly discriminating the characteristics of VeHIFs as compared to other disturbances. Harmonics could appear during other disturbances including capacitor bank and Asynchronous Machine (AsM) switching or starting a Variable-Speed Drive (VSD) controlled motor. It is critical to distinguish such disturbances from VeHIFs. In this section, authors present the method of harmonic temporal growth analysis for these three disturbances. In simulating the transient currents during the switching of a capacitor bank, a 600-kVAR 3-phase capacitor bank was modelled in a 5-bus radial 22-kV feeder. For the AsM, a 10-HP squirrel-cage induction machine was connected to the 22-kV feeder through a step-down transformer. The third modelled disturbance is a low voltage VSD controlled AC motor also connected to the feeder via a step-down transformer. In the temporal harmonic growth analysis, 20-ms sweeps (one per every 0.1 s) were used. In all three cases, switching occurs at the 0.5 s. Fig. 12 shows the analysis due to switching of the capacitor bank. As shown in Fig. 12, there is a sudden surge in all harmonic indicators post switching of the capacitor. However, these stabilise after the first sweep. A similar observation can be seen in the case of the AsM (see Fig. 13). For the VSD controlled motor (see Fig. 14), this stabilisation of the odd harmonic indicators lasts slightly longer (~1.4 s), but it still cannot replicate the unstable HIF current behaviour. In comparing the disturbances (presented in Figs. 12 to 14) to HIF currents, some key differences are observed. First of all, the odd-harmonics during the capacitor bank switching are very large in magnitude, while odd-harmonics during a VSD or AsM are more comparable in magnitude to those emitted during VeHIFs. However, the key difference is that VeHIF current odd harmonic signatures are long lasting, unstable and very random. In the case of the analysed disturbances, disturbance signatures are short-lived and instant with the core of the harmonic signatures being present only during the first few initial ms of switching. These disturbances can certainly cause LF signatures, but their short-lived nature is the key to discriminating them from VeHIFs.

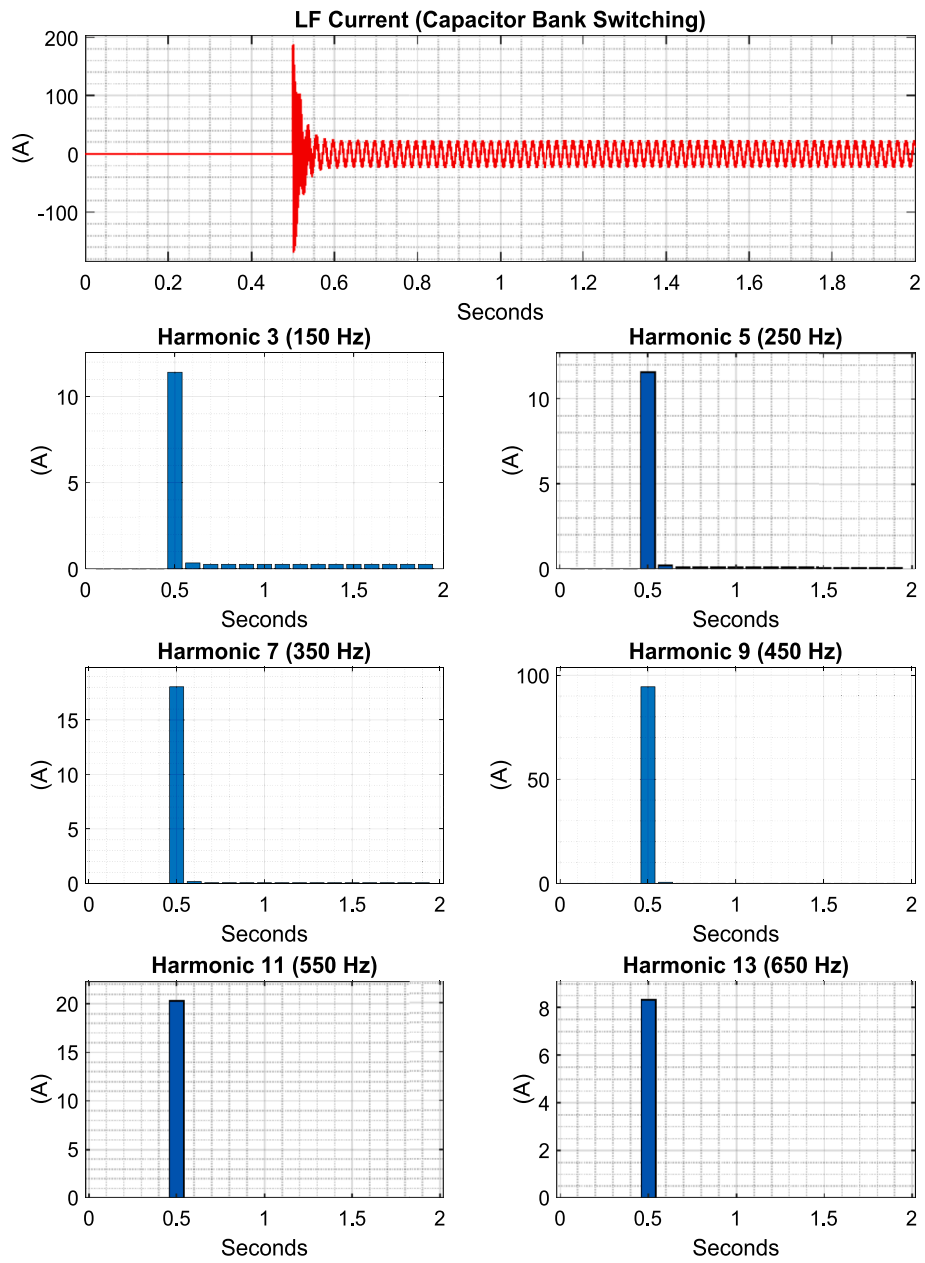


Fig. 12. Harmonic signatures during a capacitor bank switching.

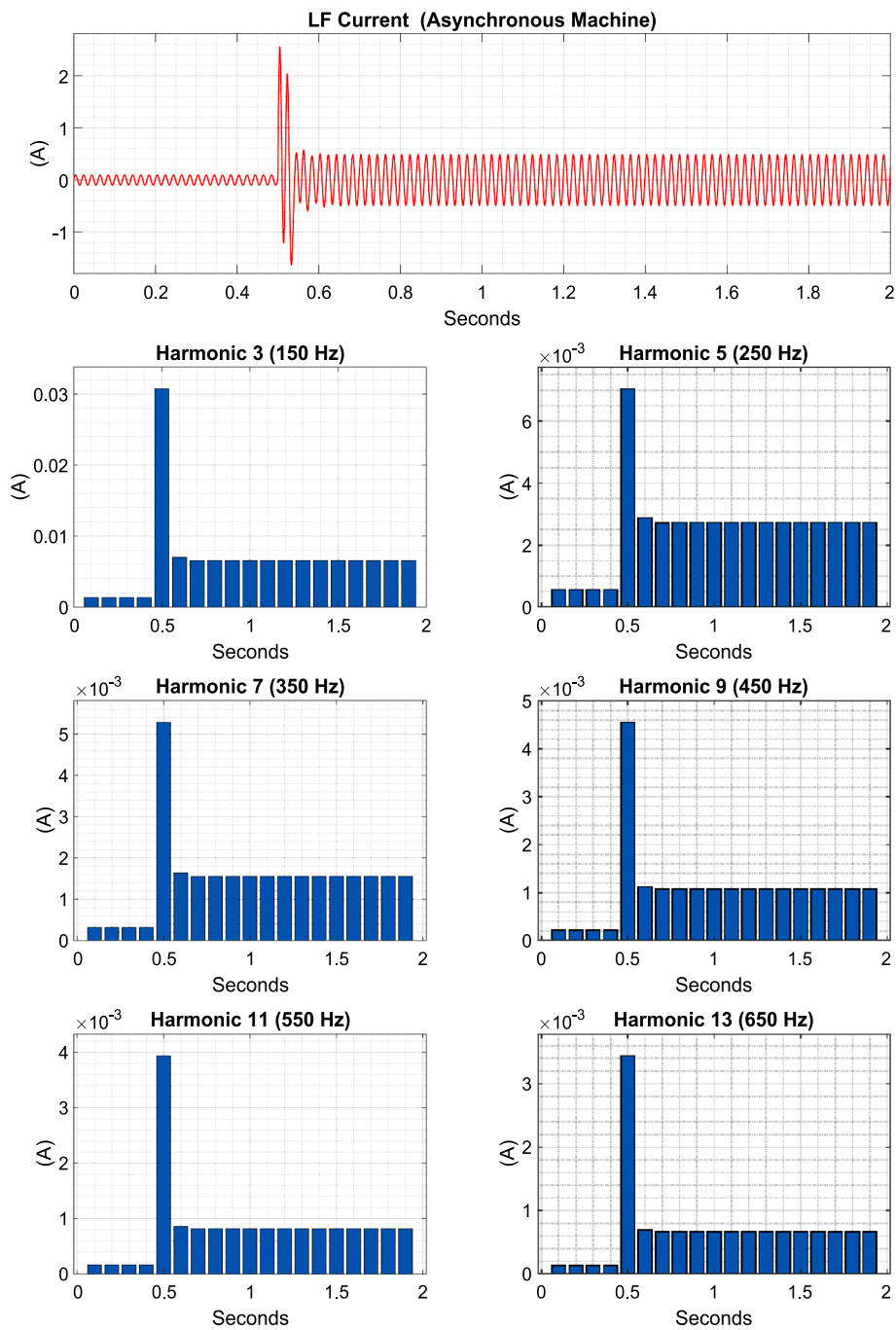


Fig. 13. Harmonic signatures during asynchronous machine switching.

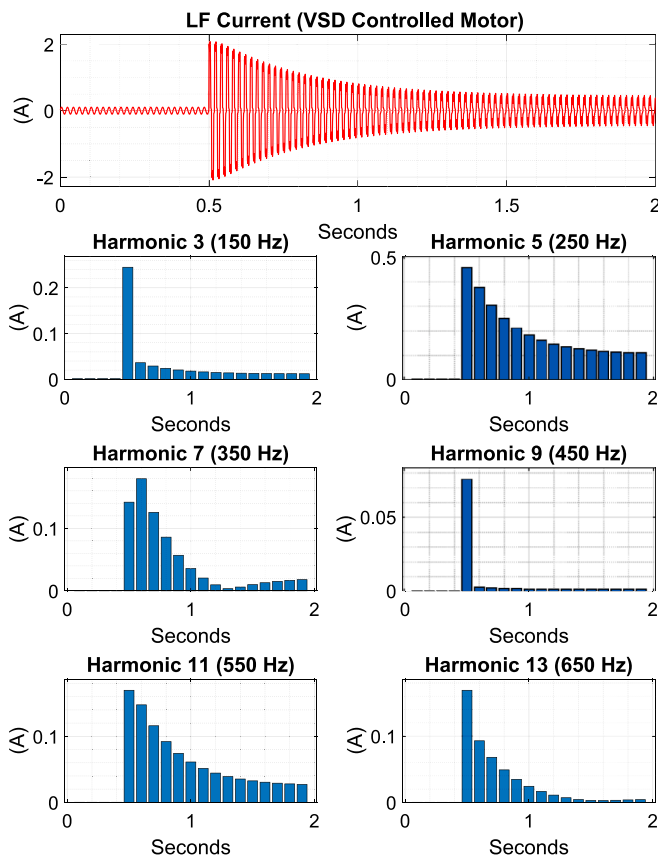


Fig. 14. Harmonic signatures during VSD controlled motor switching.

Table 7
Number of tests analysed for each species.

Species	# of Tests	Species	# of Tests
A. Meansiee	14	Eu Viminalis	13
A. Melanoxylyon	13	F. Angustifolia	12
A. Pycnantha	10	P. Undulatum	15
A. Verticillata	20	Pinus Radiate	11
C. Glaucophyllus	14	S. Molle	7
Eu. Baxteri	19	Salix Sp	8

9. ‘Big data’ analysis on the temporal averages

Generalizing research findings is not possible by analysing only two fault recordings. Accordingly, this section presents a big data analysis on the fault current odd-harmonic signature magnitude comparison of the eleven analysed species. In undertaking this analysis, 156 1-A_{rms} limit fault recordings were used composing the species and test quantities shown in Table 7. The number of tests under each species category is not the same, as authors attempted to base the results and findings on as many tests as possible within limitations of the available database (i.e. the overall test numbers were not necessarily the same for each species).

Fig. 15 shows the mean and STD analysis of all odd-harmonics using 60 sweeps from all recordings. The tests were of different durations, but all tests had at least 60 sweeps. Therefore, this analysed served to determine the dominant harmonics using 60 sweeps from each test, common to all fault recordings. This was undertaken to remove the bias of longer duration tests. As in Fig. 15, hrm₃ is the most dominant harmonic with the highest average magnitude as well as volatility. Table 8 shows the case when all of the sweeps (from all tests) were analysed. In undertaking this ‘big-data’ analysis, all temporal odd-harmonic magnitudes were first averaged across the over-fault of each test, and then the

over-fault odd-harmonic averages of the tests were used for calculating the overall means for the entire dataset. Harmonic-3 is still the leading indicator with the highest mean value and STD.

Fig. 16 compares the average hrm₃ magnitudes of all species. The mean hrm₃ current magnitude of each test was first computed (per test) over the entire fault duration and these per-test means were later further averaged for the entire test group of each species. The data points are the FFT magnitudes of odd harmonic current signatures in 20-ms sweeps as per Section 6. For example, in the case of VT343 of Fig. 11, the overall hrm₃ current magnitude mean was ~10 mA over the fault duration. From this point onwards, the term ‘over-fault’ will be used to signify statistical quantities measured using the data points from fault start to fault end. When the over-fault hrm₃ magnitude averages of all seven tests (of the S. Molle species) were averaged, this equated to 5.2 mA. As in Fig. 16, S. Molle was the species with the smallest average hrm₃ emissions. While Salix was the species with the smallest fire risk as identified in [2] (on the basis of analysis of the emitted embers), it is also the species with the least hrm₃ signature emissions. Based on this finding, S. Molle is concluded as the species with the best electrical conductivity.

In contrast, Salix (Willow), with the highest fire-risk, is the species with the largest hrm₃ emissions. Faults involving this species more likely to be cleared using odd-harmonics signatures. The average over-fault hrm₃ contribution of the Salix was 9.4 times that of the S. Molle. There clearly appears to be a link between the physical ignition processes that a species experiences during a conductor contact and the emitted harmonic signatures. Authors developed the ‘un-classification’ risk index, inversely proportional to the average hrm₃. This index represents un-classification odds of species using only odd-harmonic content variation. As in Table 9, Salix has the lowest ‘un-classification’ risk of 0.0204, while S. Molle has the highest ‘un-classification’ risk of 0.1923. As discussed earlier, low fire-risk species would still have higher odds of detection using traditional OC methods as the fault current would increase faster in vegetation contact faults involving these species. Subsequently, the un-classification risk index herein only refers to harmonic content based classification.

Fig. 17 shows the comparison of all ‘odd-harmonic’ magnitude averages. Two metrics are being used for the ‘un-classification’ risk assessment. First is the hrm₃ averages, as the highest magnitude odd-harmonic, and the second is the average of the hrm_{all} cumulative total. Based on this hrm_{all} analysis, a second ‘un-classification’ risk index has been developed by the authors, still inversely proportional to the average of the cumulative totals of all odd-harmonic current magnitudes. Table 10 shows this second un-classification risk indexation, where there is little change in the order. With the hrm₃ based risk indexation, there was a 9.42 ratio between the risk indexes of the S. Molle and Salix. In the case of the hrm_{all} based indexation, the ratio between Salix and S. Molle decreases to 5.64 signifying that hrm₃ is indeed very dominant in high fire-probability species such as the Salix.

In the hrm₃ only risk indexation, the ratio between the un-classification indexes of two most risky species, the Salix and F. Angustifolia, is ~4. This ratio declines to ~3 in the case of the hrm_{all} based indexation. When A. Verticillata and S. Molle (Peppercorn) are analysed as the two lowest risk species, one can see that the ratio between their un-classification indexes is 1.21 in the case of the hrm₃ only indexation, and 1.4 for the hrm_{all} based analysis. While S. Molle has the highest un-classification index based on its lower magnitude odd-harmonic signatures, it will later be shown that it is also the species with the fastest fault current (I_f) development. Yet, while the S. Molle species has the highest harmonics based un-classification risk, it is also the species with the highest and fastest detection odds using old-fashioned OC protection systems. In this section, authors have presented an analysis based on over-fault averages. In the following sections, the focus is on the temporal growth of the indicators. This analysis seeks to understand the growth rates in different species such that fast and slow harmonic growth species can be identified.

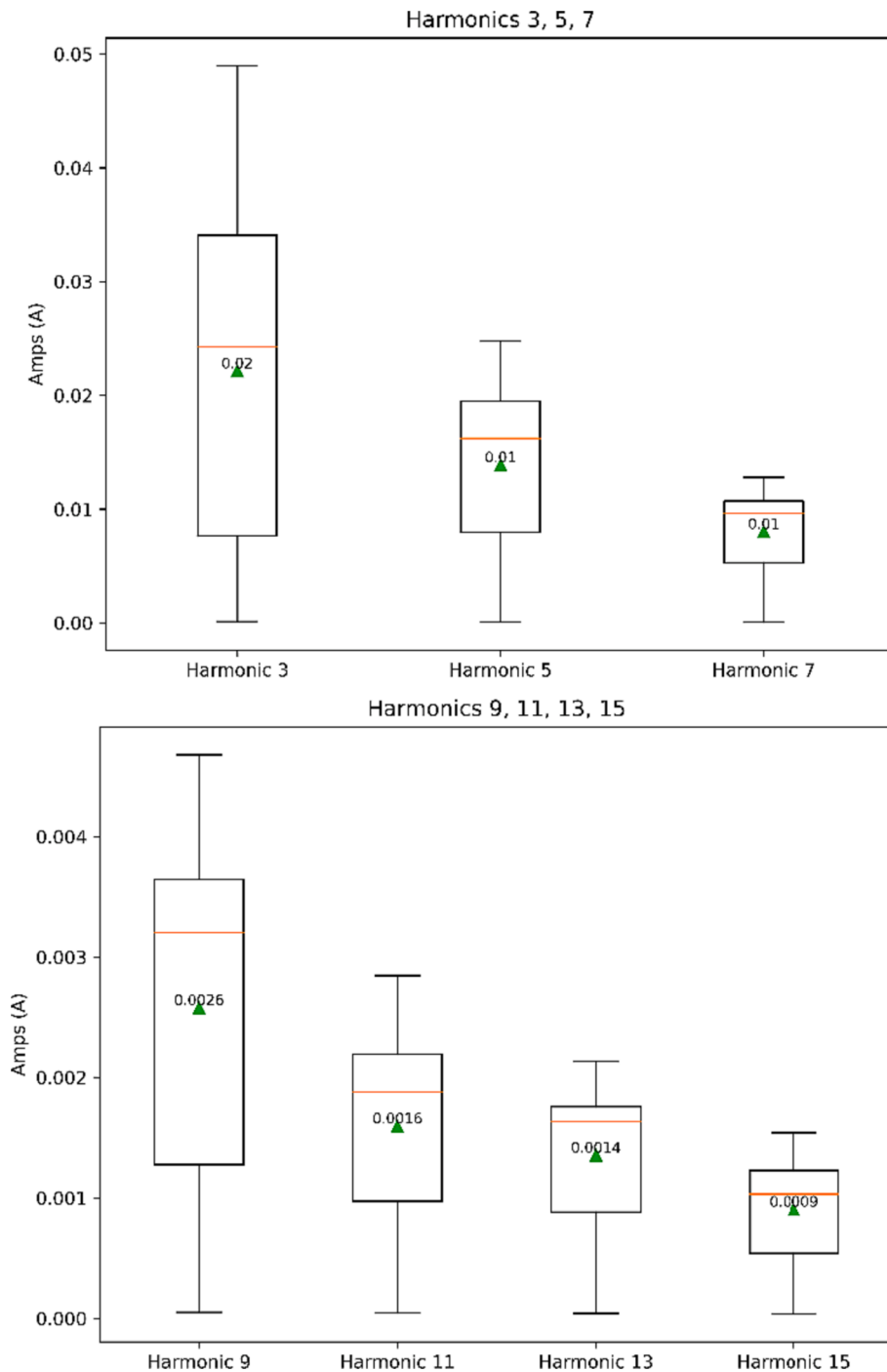


Fig. 15. Comparison of average odd-harmonic currents and their volatility using 60 sweeps from each test.

Table 8

Comparison of odd-harmonic magnitude averages and STD calculated using full durations of each test.

Harmonic #	Mean	STD
Harmonic 3	0.028191	0.018590
Harmonic 5	0.014015	0.006769
Harmonic 7	0.007126	0.002776
Harmonic 9	0.002859	0.001332
Harmonic 11	0.001907	0.000999
Harmonic 13	0.001392	0.000563
Harmonic 15	0.000990	0.000466

10. 'Big data' analysis on temporal data points

Figs. 18 and 19 show the distribution of odd harmonic current signatures. Data points are the magnitudes of odd harmonics in a data point per second procedure. In the former analysis, the focus was on the over-fault averages. This section analyses the entire data from all sweeps. Box plots are used in statistical analysis to visualize the dataset distribution. They succinctly illustrate central tendency, spread, skewness, outliers, and overall distribution. In this context, a box plot helps visualize the distribution of h_{m3} and 'harmonic averages' across different species. This supplements statistical tests by highlighting means, medians, spread, and outliers per species. In our analytics explained in Fig. 18, the species with the higher median h_{m3} values and more outliers,

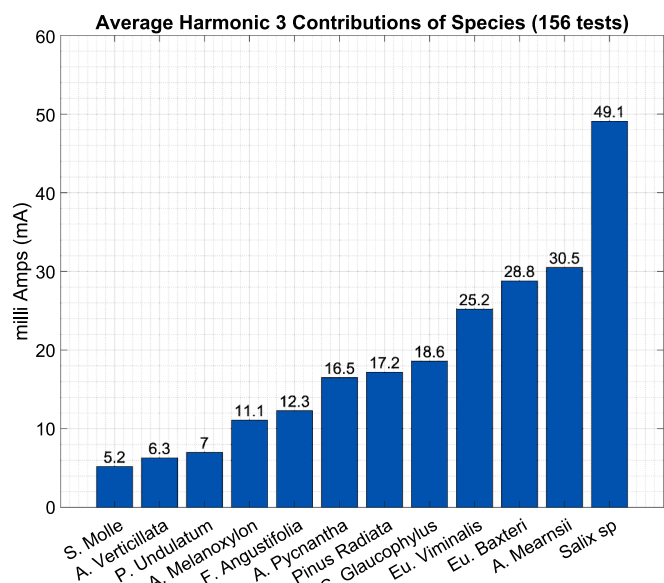


Fig. 16. Comparison of average harmonic-3 current in all species.

Table 9

Harmonic 3 magnitude based un-classification risk indexation.

Species	Risk Index 1
Salix (Willow)	0.0204
Fraxinus Angustifolia (Desert Ash)	0.0813
Acacia Mearnsii (Black Wattle)	0.0328
Pinus Radiata (Radiata Pine)	0.0581
Eucalyptus Baxteri (Stringybark)	0.0347
Eucalyptus Viminalis (Manna Gum)	0.0397
Acacia Melanoxyylon (Blackwood)	0.0901
Cotoneaster Glaucophyllus (Cotoneaster)	0.0538
Acacia Pycnantha (Golden Wattle)	0.0606
Pittosporum Undulatum (Native Daphne)	0.1429
Allocasuarina Verticillata (Drooping Sheoak)	0.1587
Schinus Molle (Peppercorn)	0.1923

particularly Salix Sp., are likely to pose a higher fire-risk, given their higher and more variable hrm_3 signatures. Species with lower and less variable hrm_3 values (e.g. F. Angustifolia) could pose lower-ignition risk in terms of charring potential and emission of embers. F. Angustifolia was the species with the second highest average fire risk in [2]. On the basis of its hrm_3 emissions based analysis alone, it presents a lower risk. There is a clear link between the harmonics signature magnitudes and the extent of volatility (a sign of charring) that a branch experiences. However, it may not be the only link. This discrepancy between the high fire-risk rating of F. Angustifolia in [2] and the lower risk determined herein (on the basis of harmonic emission magnitudes alone) have prompted us to consider other factors (such as the I_f growth rate) as well. That analysis will be presented in Section 10.

The hrm_3 appears to be a proxy for the carbonization potential of each species, and this characteristic, in turn, can be linked to the subsequent bushfire risk that a species presents. For instance, Salix has the highest median hrm_3 , suggesting it consistently experienced more carbonization than the other species. The large number of outliers for Salix suggests that there might be individual samples with significantly higher levels of harmonic emissions. The whisker below the box suggests a broad range of lower harmonic emissions as well, indicating a significant variability in this species. Then, Salix is a species of concern in conductor-to-tree contacts. Eu. Baxteri also shows a high maximum hrm_3 value, before the upper fence, indicating that there were several instances, where it experienced high harmonic signature emission due to the ignition development processes. This suggests a high VeHIF risk in

these species, although the median is lower than that of the Salix, indicating that on average, this species might pose less risk.

Species such as A. Mearnsii, Eu. Viminalis, P. Radiata show many outliers above the upper extreme line. This implies that while the majority of samples from these species pose relatively low or moderate risk, they have several instances with significantly high harmonic emissions. And hence, they may pose an intermittent, but notable bushfire risk. F. Angustifolia has the smallest box, which indicates less variability in its harmonic signatures. It also has the lowest maximum value before the upper fence, resulting in hrm_3 emissions consistently lower than other species. This species, therefore, might be least likely among those tested to cause ember formation during a VeHIF. Key statistical measures including the mean, STD, skewness, kurtosis, and maximum values of these signatures have been computed for each species. The species Salix Sp. exhibits the highest mean odd harmonic current signature across all harmonic indices from hrm_3 to hrm_{15} . This suggests a consistent presence of heightened harmonic levels for this species. Contrarily, S. Molle registers the lowest mean values across the majority of harmonic indices, indicating relatively lower levels of harmonic signals in comparison.

Variability in the harmonic signatures is revealed through the STD values. Both Salix Sp. and A. Mearnsii present high STDs, reflecting a broad dispersion of harmonic indices and implying a higher degree of variability in their harmonic signals. Conversely, the S. Molle and A. Verticillata species present lower STDs. This is indicative of tighter clustering of harmonic indices around the mean and hence, a higher level of consistency in their harmonic signals. Skewness, which measures the asymmetry of the distribution, divulges interesting insights. Both A. Verticillata and F. Angustifolia exhibit high skewness in most harmonics, with heavily skewed and asymmetric distributions. In contrast, Salix, A. Pycnantha, and Eu. Baxteri manifest less skewness, implying their harmonic distributions are more symmetrically dispersed. A. Verticillata and F. Angustifolia further stand out with their very high kurtosis values, suggestive of a sharp-peaked and leptokurtic distribution with more outliers or extreme values. Meanwhile, Salix and C. Glaucophyllus display lower kurtosis values, indicating a more platykurtic or normal distribution with fewer outliers. Fig. 19 compares hrm_{all} averages of all sweeps (from all tests) of particular species. For example, for F. Angustifolia, 1853 sweeps from 12 tests were used.

The max values provide insights into the harmonics' extremes. F. Angustifolia and A. Mearnsii have the highest max values in most harmonic indices, denoting the presence of relatively high harmonic extremes. The harmonic current analysis highlights significant disparities among the various plant species. Salix typically exhibits the strongest harmonic signals with the highest mean and max harmonic indices. In contrast, S. Molle generally displays weaker harmonic signals with the lowest harmonic indices. These discrepancies could be attributed to the biological or structural variances among the species, providing a potential basis for species identification or classification. These findings underscore relevance of electrical studies in elucidating the unique characteristics of different species through the analysis of harmonic signatures. Our comprehensive analysis encompassed several statistical computations for the harmonic indices of each plant species. These are the skewness, mean, STD, kurtosis, min and max values are in Fig. 20. These measures, each calculated individually for each harmonic index of each species, offered a nuanced understanding of the unique harmonic signatures of the investigated species. For instance, skewness quantified the asymmetry extent and direction in the probability distribution of the harmonic indices. The mean values indicated the central tendency, and the STD portrayed the dispersion (variability) around the mean. Moreover, the max and min values provided the range of these harmonic indices. The intricate interplay of these statistical measures collectively offered an understanding of the harmonic current signatures' behavior within and across different species. A detailed representation of these computations for each species for the hrm_{all} averages is visually presented in Fig. 20. Table 11 compares the average fire-risk in [2] against

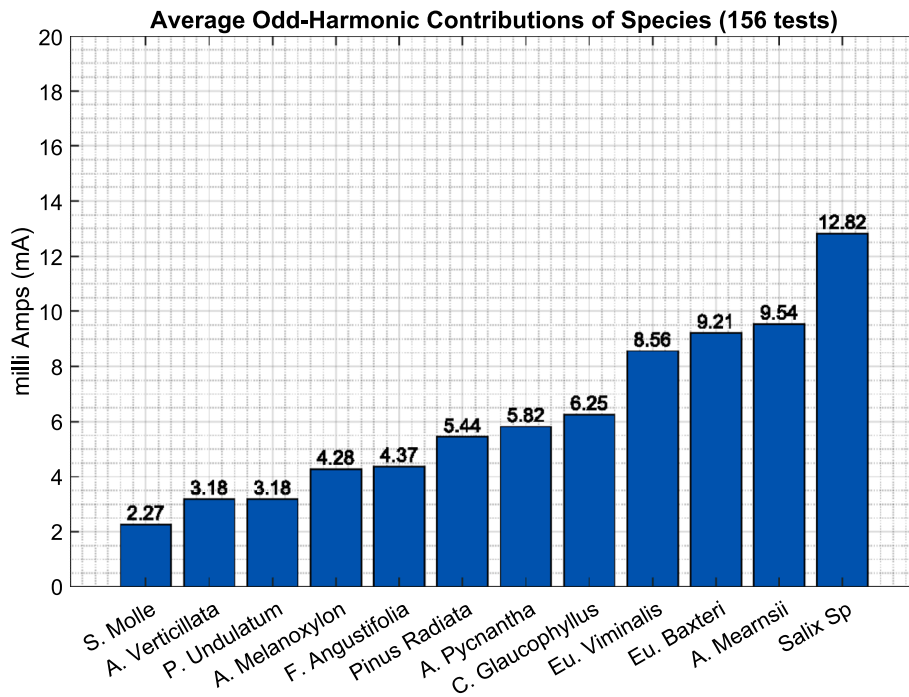


Fig. 17. Comparison of all odd-harmonic current averages of the species.

Table 10

All odd-harmonics' magnitude average based un-classification risk indexation.

Species	Risk Index 2
Salix (Willow)	0.0780
Fraxinus Angustifolia (Desert Ash)	0.2288
Acacia Mearnsii (Black Wattle)	0.1048
Pinus Radiata (Radiata Pine)	0.1838
Eucalyptus Baxteri (Stringybark)	0.1086
Eucalyptus Viminalis (Manna Gum)	0.1168
Acacia Melanoxyllon (Blackwood)	0.2336
Cotoneaster Glaucohyllus (Cotoneaster)	0.1600
Acacia Pycnantha (Golden Wattle)	0.1718
Pittosporum Undulatum (Native Daphne)	0.3145
Allocasuarina Verticillata (Drooping Sheoak)	0.3145
Schinus Molle (Peppercorn)	0.4405

the risk assessment based on the computational method herein. In [2], the 'fire probability ranking' was an outcome of the size, temperature, and amount of embers as well as how long they kept glowing. The rules were applied by reviewing infrared videos produced by a thermal camera, which was focused on the test rig floor [2]. The intent herein has been to perform a similar assessment based on the analysis of odd-harmonic signatures emitted from the species. Our hypothesis is that high fire-risk species are poorer conductors of electricity and emit larger amounts of odd-harmonic signatures, when exposed to ph-to-e conductor contacts.

It also follows that lower fire-risk species are better electricity conductors, and thus emit less signatures, when exposure to the same HIFs. The computational method described herein relies on assessment of the over-fault (i.e. over the full duration of a test) odd-harmonic current magnitudes. For example, Table 11 ranks the species in terms of their mean odd-harmonics averages. This is calculated by estimating the average of the over-fault harmonic indices (hrm_3 to hrm_{15}) of each test of a particular species. Then, a cumulative sum of the indices is taken to calculate the overall mean odd-harmonics average. The fire probability rank percentages are then calculated by normalizing the mean odd-harmonics averages by that of the Salix (which has the highest odd-harmonic average). As shown in Table 11, there are similarities in the

rankings of the two methods, especially for the highest risk and the lowest risk bands. The highest risk species, Salix, is common in both rankings. The lowest risk species (P. Undulatum, A. Verticillata, and S. Molle) are also the same in both rankings. There are some ranking differences in the mid-tier species. This may perhaps be attributed to the human errors in the manual visual analysis of the infrared videos produced by the thermal camera in [2], or perhaps to the consideration of only the mean odd-harmonics averages herein. For example, when the species were ranked herein on the basis of the multiplicand of their mean and maximum odd-harmonics averages, an improvement in the ranking of the mid-tier species can be seen (see Table 12).

11. 'Big data' analysis on temporal growth rates

This section compares the temporal signature growth rates of species based on the all odd harmonics averages. In undertaking this analysis, the hrm_{all} magnitudes were first summed per sweep and this data was used for the temporal growth analysis. While hrm_3 is dominant, this approach enabled the team to take into account a wider spectrum of indicators, than solely on the hrm_3 .

Table 13 shows the average sweep numbers (#) when the hrm_{all} magnitudes reached their respective maximums in various species as well as half of these max amplitudes. The computation was carried out by first calculating the total odd-harmonics signature and then identifying at which sweeps it reaches its maximum value and half of this maximum. Finally, the average sweep index for a species was calculating by taking the average of the individual sweep indexes (when the total hrm_{all} contribution was @ its max) of the individual tests that fall under a particular species. A similar analysis is conducted to determine the average sweep index when a particular species reached half of its odd-harmonic signature max. As discussed previously, the frequency-domain based FFT magnitudes of all fifteen odd-harmonic current signatures were calculated using 20-ms sweeps, repeated once a second. Therefore, a sweep equates to a full second.

The temporal growth speeds were then calculated (see Table 14) by normalizing the average sweep numbers in Table 13 to the average sweep numbers of F. Angustifolia (i.e. the species where slowest growth occurs). This enables us to compare and contrast the species in terms of

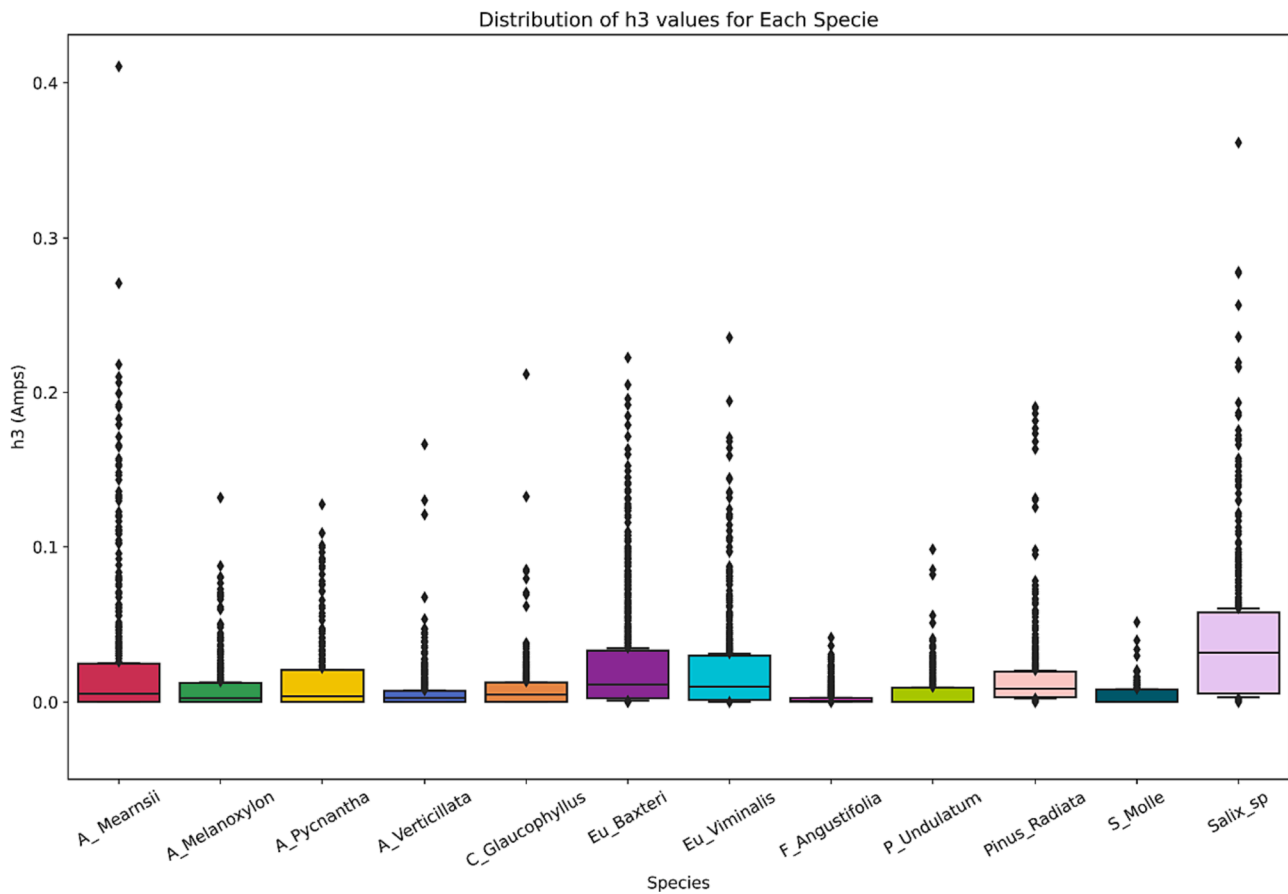


Fig. 18. Distribution of individual hrm_3 values for each species.

their odd-harmonic current signature growth rates. As shown in Table 14, S. Molle has the fastest speed of reaching its odd-harmonics average maximum due to faster fault current development in this species. P. Undulatum, on the other hand, has the fastest speed to its max/2 mark. In both categories, F. Angustifolia had the lowest speed. Some vegetation species such as F. Angustifolia require further discussion, after the analysis of their temporal growth rates. Even though F. Angustifolia was the species with the 2nd highest average fire-risk based on ember formation in [2]. In the earlier analysis herein, however, it appeared to have a lesser risk on the basis of its harmonic emission magnitudes alone. This suggests that the speed of temporal growth of harmonic signatures might be as critical as the average magnitude of emissions. Specifically, the slow growth of I_f (and correspondingly the slow growth in harmonic signatures) in a species (e.g. F. Angustifolia) may still compensate against the low-magnitude harmonic averages and still cause a relatively high fire-risk. The species of P. Radiata is a second critical example to this new observation. In the former analysis based on harmonic contents alone, Pinus Radiata was ranked as the 7th highest fire-risk species (against its 4th ranking in [2]). As shown in Table 14, P. Radiata has the 2nd slowest temporal growth, after F. Angustifolia. This confirms that a fire-risk analysis based on the magnitude of harmonic signatures alone is not sufficient, and the temporal growth rate is also a factor. Fig. 21 shows the temporal growth comparison of the average of hrm_{all} . In undertaking the following analysis, the sweep by sweep hrm_{all} temporal averages were calculated and plotted for each species. Fig. 21 shows the temporal growth comparison of the species with the odd-harmonics averaged per sweep. In plotting the data in Fig. 21 the odd-harmonics totals were first calculated on a sweep-by-sweep for each tests of a species, and the odd-harmonics totals were then averaged for each species category. The slow temporal growth in F. Angustifolia can also be clearly seen in Fig. 21.

The key rationale in this analysis was to identify species where I_f (and the accompanying harmonics) would grow the fastest and the slowest to their test maximums. This is significant as harmonic emission magnitudes are alone inadequate in representing the precise fire-probability risk of a species. Another key factor, the speed of growth, had to be considered using a big-data analysis of 156 tests such that generalizations could be made, rather than making conclusions on the basis of a handful tests.

12. ANOVA and Tukey HSD tests

For addressing the outlined research questions regarding the effects of different vegetation species on odd harmonic current signatures and potential implications for the fire and un-classification risks, authors have developed a comprehensive analytical approach. This research builds upon the existing literature, such as Marxsen [2], suggesting that rapid detection of earth faults can significantly reduce fire risks. The primary dependent variable was the ‘average_harmonic’ encapsulating the magnitude and temporal growth of odd harmonic current signatures. This variable provides insights into the conductivity of different vegetation species under conditions indicative of High-Impedance faults (HIFs). As discussed above species, with higher conductivity, were observed to generate less harmonic current signatures. The investigation discussed herein involved a diverse range of vegetation species, each with distinct physical characteristics and conductivity properties, making them appropriate candidates for the study. These were encoded in our model as a categorical variable, ‘species’. Authors initially applied an Analysis of Variance (ANOVA) test to evaluate the hypothesis that the ‘average_harmonic’ is the same across all species. The results revealed a highly significant effect of the analysed species on the ‘average_harmonic’, with a p-value of $7.322032e-148$. This is far below the

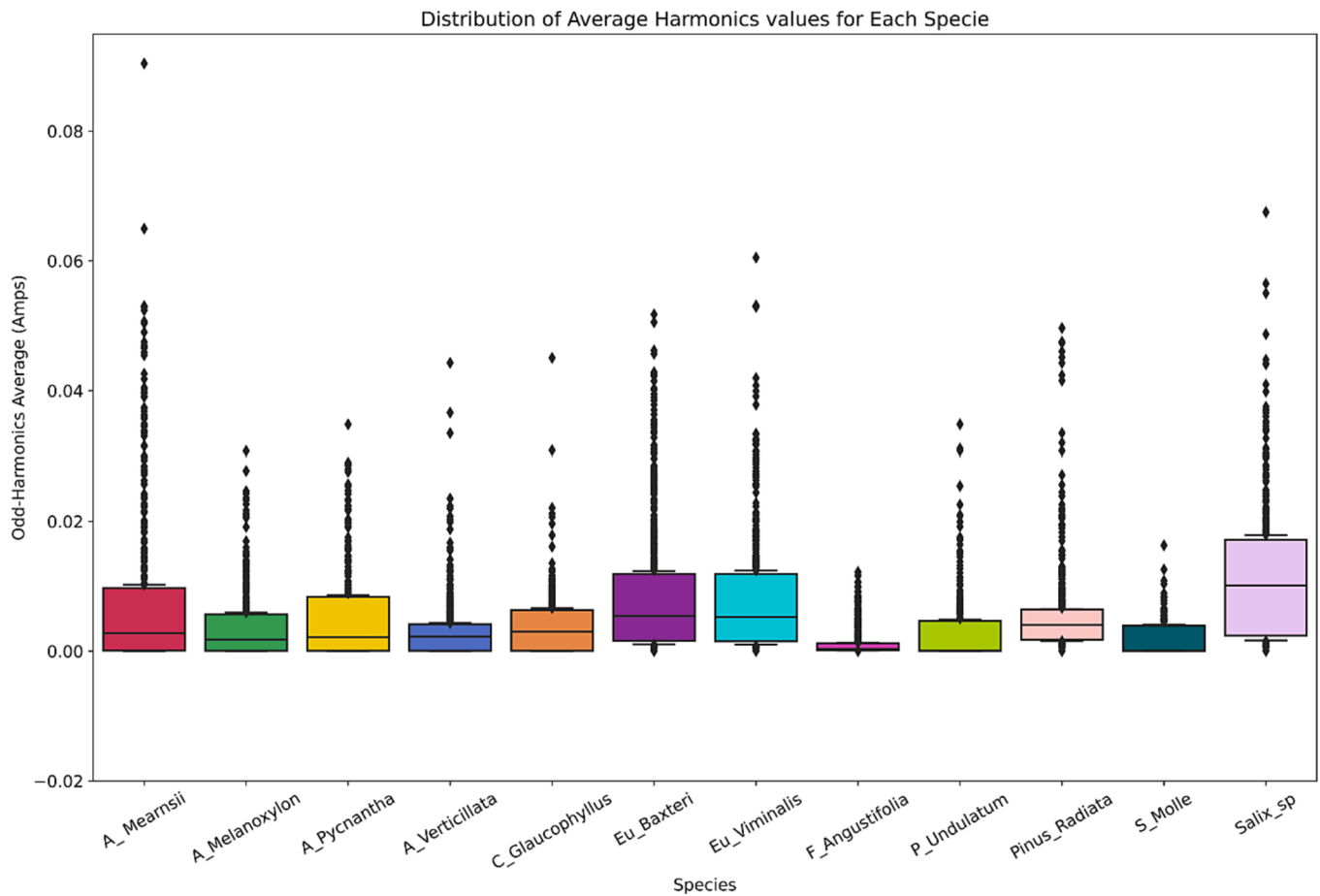


Fig. 19. Distribution of individual odd-harmonic averages values for each species.

conventional 0.05 threshold for statistical significance. This finding rejects the null hypothesis, confirming that there are indeed significant differences in the 'average_harmonic' among the tested vegetation species.

However, the ANOVA test only tells us that not all species produce the same 'average_harmonic'; it does not specify which species differ from each other. Therefore, authors then applied a post-hoc Tukey Honestly Significant Difference (HSD) test [24] to perform pairwise comparisons of all species. The results of the Tukey HSD test confirmed that the effect of species on the 'average_harmonic' is heterogeneous; in other words, the differences in harmonic signatures are not uniform across all species pairs. Explicitly, certain species pairs showed significantly different harmonic signatures, as indicated by p-values below 0.05 and a 'True' value in the reject column. For instance, the pairs 'A_Mearnsii' and 'A_Melanoxyilon' showed a significant difference with a mean difference of -0.0053 and a p-value of 0.001. On the contrary, other species pairs, such as A. Mearnsii and Eu. Baxteri, showed no significant difference in their harmonic signatures, with a p-value of 0.9 and a 'False' value in the reject column. In other words, these two species were close to each other from the viewpoint of odd-harmonic fault current signatures and current conductivity. This nuanced understanding of species' effects on the average_harmonic allows us to make a more informed assessment of their respective fire risks and detection challenges. In turn, this could guide utilities on implementing more effective vegetation management strategies, ensuring the safety and affordability for the power distribution industry and communities. For instance, species with high 'average_harmonic' may be classified as 'high-fire probability', warranting their maximum clearance in bushfire-prone areas, while species with lower average_harmonic could be considered 'low-fire probability' and managed accordingly. Besides, the temporal

growth speed comparison of odd-harmonic signatures across different species provides insights into the potential speed of detection possible for earth faults in different vegetation. This information is crucial for effective and swift risk management strategies aiming to minimize the fire risk associated with vegetation-induced HIFs.

Yet, the complexity and diversity of species' effects on the average_harmonic necessitate further research to fully understand and categorize the potential fire and detection risks associated with different species. For example, lower average_harmonic species are good electric conductors and may need to be further tested to develop better strategies in dealing with them. One weakness of the project in [1] was the fact that the tests were terminated early as the fault current reached the pre-set limits of 0.5, 1, and 2 A_{rms} . As such, the fault tests of good conductivity species (e.g. S. Molle and P. Undulatum) were concluded fast, without getting the full picture on the effects of sustained high fault current amplitudes on these. Future research on these 'low-fire probability' species is advisable to better understand the extent of uninterrupted fault current development potential and whether they would eventually experience break-out of flames leading to charring (when subjected to high fault currents for many minutes). In conclusion, our research represents an important step in bridging the knowledge gap in this area, with potential implications for effective risk mitigation and vegetation management.

Further building on our examination of the 'average_harmonic', we also conducted a parallel analysis for another dependent variable: 'harmonic_3'. This variable, like the 'average_harmonic', captures aspects of the odd harmonic current signatures, allowing for an additional layer of comparative analysis. The ANOVA results for both variables (average_harmonic and harmonic_3) suggest a highly significant effect of species on the respective harmonic signatures. Notably, the F value

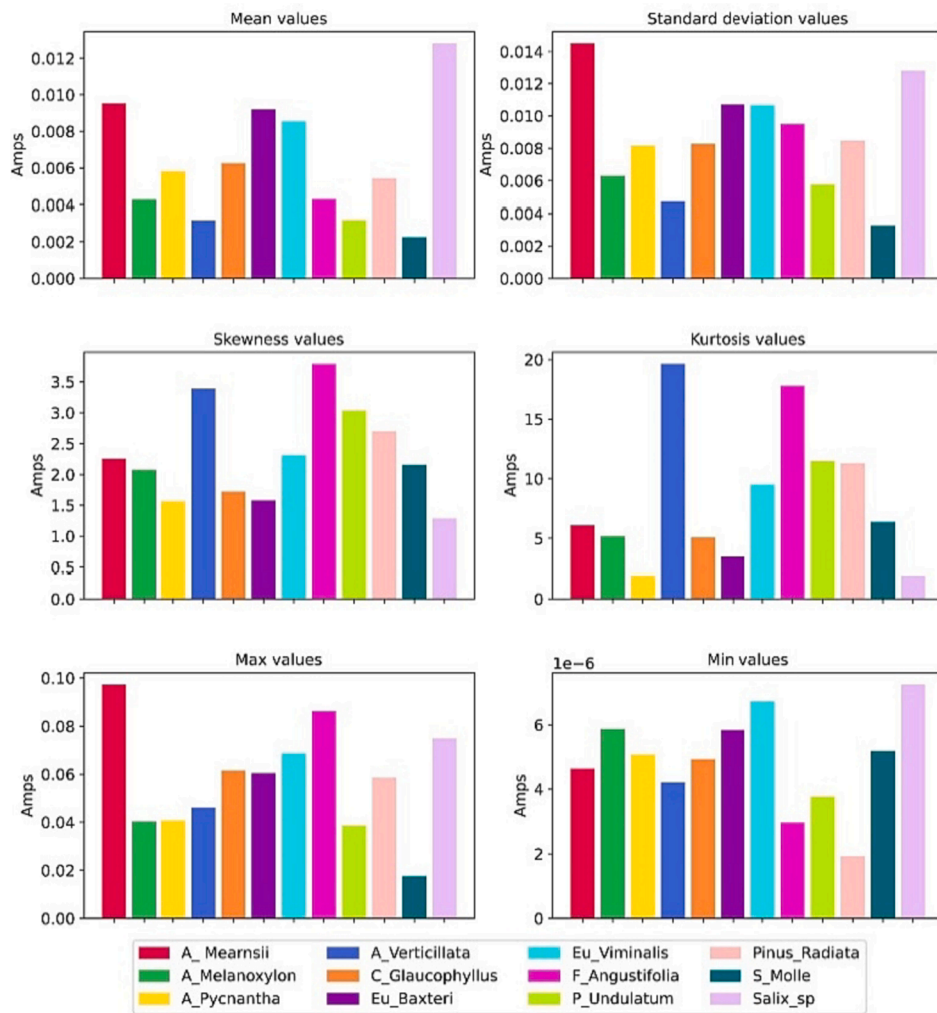


Fig. 20. Statistical metrics of the odd-harmonics average across the species.

Table 11
Fire risk categorization based on the mean odd-harmonics averages.

Species	Average Fire Probability & Rank [2]	Fire Risk Probability % & Rank
Salix	1 (# 1 in [2])	100 (# 1)
Acacia Mearnsii	0.57 (# 3 in [2])	74.44 (# 2)
Eucalyptus Baxteri	0.53 (# 5 in [2])	71.87 (# 3)
Eucalyptus Viminalis	0.5 (# 6 in [2])	66.78 (# 4)
Cotoneaster Glaucophyllus	0.21 (# 8 in [2])	48.78 (# 5)
Acacia Pycnantha	0.1 (# 9 in [2])	45.4 (# 6)
Pinus Radiata	0.55 (# 4 in [2])	42.42 (# 7)
Fraxinus Angustifolia	0.58 (# 2 in [2])	34.11 (# 8)
Acacia Melanoxyylon	0.23 (# 7 in [2])	33.38 (# 9)
Pittosporum Undulatum	0.07 (# 10 in [2])	24.83 (# 10)
Allocauarina Verticillata	0.05 (# 11 in [2])	24.8 (# 11)
Schinus Molle	0 (# 12 in [2])	17.67 (# 12)

and the p-value (PR(>F)) for harmonic_3 are even more pronounced than those for the average_harmonic. For harmonic_3, the F value is 76.91, and the p-value is extremely close to zero (1.89 x 10⁻¹⁶⁵). This suggests that the effect of species on the harmonic_3 is more pronounced compared to the average_harmonic. This insight contributes to a more nuanced understanding of how different vegetation species might influence distinct aspects of odd harmonic current signatures, with

Table 12
Fire risk categorization based on the multiplicand of the mean and maximum of the hrm_{all} average.

Species	Average Fire Probability & Rank [2]	Fire Risk Probability % & Rank
Salix (Willow)	1 (# 1 in [2])	100 (# 1)
Acacia Mearnsii	0.57 (# 3 in [2])	96.72 (# 2)
Eucalyptus Viminalis	0.5 (# 6 in [2])	61.17 (# 3)
Fraxinus Angustifolia	0.58 (# 2 in [2])	38.68 (# 6)
Eucalyptus Baxteri	0.53 (# 5 in [2])	57.96 (# 4)
Cotoneaster Glaucophyllus	0.21 (# 8 in [2])	40.04 (# 5)
Pinus Radiata	0.55 (# 4 in [2])	33.2 (# 7)
Acacia Pycnantha	0.1 (# 9 in [2])	24.68 (# 8)
Acacia Melanoxyylon	0.23 (# 7 in [2])	17.96 (# 9)
Allocauarina	0.05 (# 11 in [2])	15.26 (# 10)
Verticillata		
Pittosporum	0.07 (# 10 in [2])	12.79 (# 11)
Undulatum		
Schinus Molle	0 (# 12 in [2])	4.15 (# 12)

potential implications for both fire risk and detection feasibility.

To understand which species pairs showed significantly different harmonic signatures, we again performed Tukey’s HSD tests for pairwise comparisons. The outcomes showed variations in mean differences (‘meandiff’) between species groups across the two variables. For instance, the mean difference between ‘A. Mearnsii’ and ‘A.

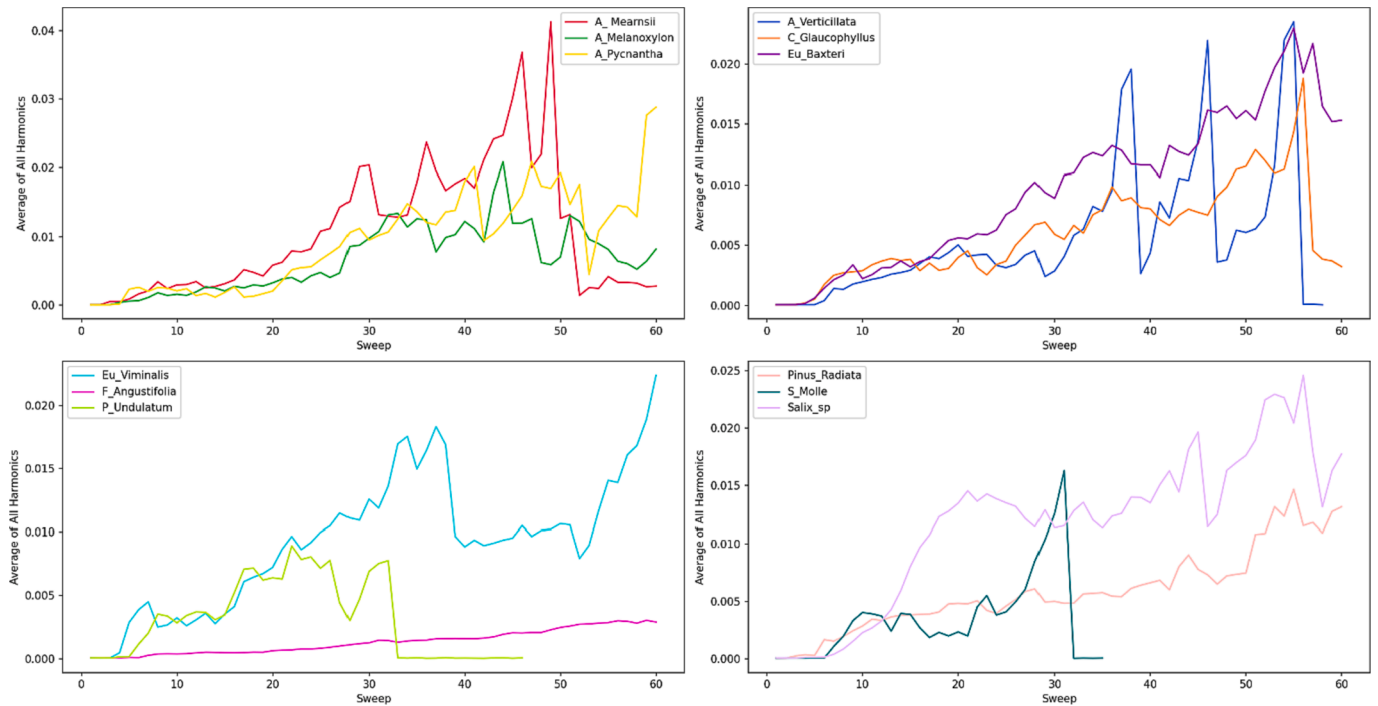


Fig. 21. Temporal growth comparison of average of all ‘odd-harmonics’ values in the species.

Table 15
Final fire-risk probability ranking of species.

Species	Fire Risk Probability % (mean × max) Rank1	Full Amp Speed (s/s) Rank2	Final Risk Probability and Rank (Rank1/ Rank2)
Salix (Willow) (# 1 in [2])	100	1.842	54.29 (# 1)
F. Angustifolia (# 2 in [2])	38.68	1	38.68 (# 2)
A. Mearnsii (# 3 in [2])	96.72	4.002	24.17 (# 3)
P. Radiata (# 4 in [2])	33.2	2.027	16.38 (# 6)
E. Baxteri (# 5 in [2])	57.96	2.79	20.70 (# 4)
E. Viminalis (# 6 in [2])	61.17	3.23	18.92 (# 5)
A. Melanoxyylon (# 7 in [2])	17.96	5.203	3.45 (# 9)
C. Glaucophyllus (# 8 in [2])	40.04	3.87	10.35 (# 7)
A. Pycnantha (# 9 in [2])	24.68	6	4.11 (# 8)
P. Undulatum (# 10 in [2])	12.79	8.03	1.59 (# 11)
A. Verticillata (# 11 in [2])	15.26	4.9	3.10 (# 10)
S. Molle (# 12 in [2])	4.15	8.059	0.51 (# 12)

harmonic emissions in faults involving this species. F. Angustifolia was ranked #6 in Table 12 on the basis of the mean/max of its hrm_{all} averages. Now, when its slow temporal growth speed is considered, its rank increased to #2, which better aligns its rank with that in [2]. In Table 12, E. Viminalis was the third highest ranked species on the basis of the mean and max of its hrm_{all} averages. By inversely considering its temporal growth speed, its rank has now dropped to #5, which also better aligns with that in [2]. The results confirm that an analytical methodology based on magnitudes of the average and maximum of odd-

harmonic signatures and a consideration of the temporal growth speed of harmonics can reliably be used for a potential estimate of a species fire-risk probability rating.

14. Conclusions

Key contribution is on the fire-risk ranking of vegetation species in VeHIF events. Odd-harmonics current signature magnitudes and the speed of temporal growth of those signatures were used as deterministic factors. Most species experience few stages of ignition development during a VeHIF. From a fire-risk perspective, the stage of charring, often accompanied by a breakout of flames, is the most critical. High-risk species were those that experienced volatile fault currents and higher levels of odd-harmonic signature emissions during charring. Intermittent arcing was also observed to be higher in high-risk species with volatile fault currents. Species with low carbonization are the lower risk ones, and they release fewer odd-harmonics signatures. While analysing the link between arcing and fire-risk, authors discovered that the V-I characteristic temporarily shifts (as arcing increases) from a linear relationship to one resembling a skewed figure-eight. While this figure-eight V-I pattern was previously reported in the literature, the temporal shift in the V-I pattern is only this explicitly validated herein. This study has also determined that the overall risk is inversely correlated with the temporal growth speed of harmonic signatures. Species with slow fault current growth also experience slow temporal growth of harmonic signatures. This elevates the fire-risk, even despite low harmonic emissions. In contrast, species with fast fault current development impose lower risks. This is due to the fault current increasing to levels, where faults may be detected by traditional overcurrent methods, before the branch catches sustained fire, with fully developed ember production. The analytical fire-risk ranking method, key contribution herein, led to findings largely compatible with observatory analysis of the fire-risk based on ember formation. Species characteristics, such as branch size and environmental factors such as humidity were out of scope of this study and can be considered in future works.

CRedit authorship contribution statement

Cagil Ozansoy: Conceptualization, Formal analysis, Investigation, Methodology, Project administration. **Omid Ameri Sianaki:** Data curation, Formal analysis.

Declaration of competing interest

The authors declare that they have no known competing financial interests or personal relationships that could have appeared to influence the work reported in this paper.

Data availability

Link to the data source available in the References

References

- [1] Victorian Government. Powerline bushfire safety program - vegetation conduction ignition test report and data. <https://discover.data.vic.gov.au/dataset/powerline-bushfire-safety-program-vegetation-conduction-ignition-test-report> (accessed 22 July 2019).
- [2] Marxsen T. Vegetation conduction ignition test report - final. Marxsen Consulting Pty Ltd; 2015. Accessed: Nov-2016. [Online]. Available: <https://discover.data.vic.gov.au/dataset/powerline-bushfire-safety-program-vegetation-conduction-ignition-test-report>.
- [3] Goodfellow J, Crudele D. Optimal design of overhead distribution systems – understanding touch potential risks due to tree-to-conductor contacts on distribution circuits. Electric Power Research Institute. Report No 1016219, December 2007.
- [4] Goodfellow J, Crudele D. Overhead distribution vegetation challenges: touch potential voltage at ground level and aloft in trees contacting energized distribution conductors. Palo Alto, CA: Electric Power Research Institute. Report No 1018463, December 2008.
- [5] Wischkaemper JA, Benner CL, Russell BD. Electrical characterization of vegetation contacts with distribution conductors - investigation of progressive fault behavior. In: 2008 IEEE/PES transmission and distribution conference and exposition, 21–24 April 2008; 2008. p. 1–8. doi: 10.1109/TDC.2008.4517149.
- [6] González P, Romero E, Miñambres VM, Guerrero MA. Experimental tests of high impedance faults in MV rural distribution network. In: 2014 International conference on optimization of electrical and electronic equipment (OPTIM), 22–24 May 2014; 2014. p. 1–10. doi: 10.1109/OPTIM.2014.6851019.
- [7] Carpenter M, Hoard RR, Bruton TD, Das R, Kunsman SA, Peterson JM. Staged-fault testing for high impedance fault data collection. In: 58th Annual conference for protective relay engineers, 2005, 5– April 2005; 2005. p. 9–17. doi: 10.1109/CPRE.2005.1430417.
- [8] Daqing H. Detection of high-impedance faults in power distribution systems. In: 2007 Power systems conference: advanced metering, protection, control, communication, and distributed resources, 13–16 March 2007; 2007. p. 85–95. doi: 10.1109/PSAMP.2007.4740902.
- [9] Chaitanya BK, Yadav A, Pazoki M. An intelligent detection of high-impedance faults for distribution lines integrated with distributed generators. IEEE Syst J 2020;14(1):870–9. <https://doi.org/10.1109/JSYST.2019.2911529>.
- [10] Shu H, Li B. Research on fault line detecting based on empirical mode decomposition (EMD) in resonant grounded systems. In: 2009 Asia-Pacific power and energy engineering conference, 27–31 March 2009; 2009. p. 1–5. doi: 10.1109/APPEEC.2009.4918686.
- [11] Slater J, Nesbitt A, Morison G, Boreham P, Conner S. Application of empirical mode decomposition in identifying key frequencies for EMI diagnostic measurements. In: 2018 53rd International universities power engineering conference (UPEC), 4–7 Sept. 2018; 2018. p. 1–5. doi: 10.1109/UPEC.2018.8541987.
- [12] Yao W, Gao X, Wang S, Liu Y. Distribution high impedance fault detection using the fault signal reconstruction method. In: 2019 IEEE 3rd conference on energy internet and energy system integration (EI2), 8–10 Nov. 2019; 2019. p. 2573–7. doi: 10.1109/EI247390.2019.9061798.
- [13] Lima É, Junqueira C, Brito N, Souza B, Coelho R, Medeiros H. A new high impedance fault detection method based on the short-time Fourier transform. IET Gener Transm Distrib 2018;12. <https://doi.org/10.1049/iet-gtd.2018.0093>.
- [14] Gautam S, Brahma SM. Detection of high impedance fault in power distribution systems using mathematical morphology. IEEE Trans Power Syst 2013;28(2): 1226–34. <https://doi.org/10.1109/TPWRS.2012.2215630>.
- [15] Cui Q, El-Arroudi K, Weng Y. A feature selection method for high impedance fault detection. IEEE Trans Power Del 2019;34(3):1203–15. <https://doi.org/10.1109/TPWRD.2019.2901634>.
- [16] Jeerings DJ, Linders JR. Unique aspects of distribution system harmonics due to high impedance ground faults. IEEE Trans Power Del 1990;5(2):1086–94. <https://doi.org/10.1109/61.53126>.
- [17] Wang S, Dehghanian P. On the use of artificial intelligence for high impedance fault detection and electrical safety. IEEE Trans Ind Appl 2020;56(6):7208–16. <https://doi.org/10.1109/TIA.2020.3017698>.
- [18] Ozansoy C, Gomes DPS. Electrical and physical characterization of earth faults for diverse bush species. Eng Sci Technol, Int J 2020;23(5):1109–17. <https://doi.org/10.1016/j.jestch.2020.03.002>.
- [19] Gomes DPS, Ozansoy C. High-impedance faults in power distribution systems: a narrative of the field's developments. ISA Trans 2021;118:15–34. <https://doi.org/10.1016/j.isatra.2021.02.018>.
- [20] Ozansoy C. VeHIF current arcing, volatility and vegetation ignition development: an EMD based volatility analysis for earth-fault classification. Eng Sci Technol, Int J 2023;48:101561. <https://doi.org/10.1016/j.jestch.2023.101561>.
- [21] Sultan AF, Swift GW, Fedirchuk DJ. Detecting arcing downed-wires using fault current flicker and half-cycle asymmetry. IEEE Trans Power Del 1994;9(1):461–70. <https://doi.org/10.1109/61.277718>.
- [22] Emanuel AE, Cyganski D, Orr JA, Shiller S, Gulachenski EM. High impedance fault arcing on sandy soil in 15 kV distribution feeders: contributions to the evaluation of the low frequency spectrum. IEEE Trans Power Del 1990;5(2):676–86. <https://doi.org/10.1109/61.53070>.
- [23] Michalik M, Rebizant W, Lukowicz M, Seung-Jae L, Sang-Hee K. High-impedance fault detection in distribution networks with use of wavelet-based algorithm. IEEE Trans Power Del 2006;21(4):1793–802. <https://doi.org/10.1109/TPWRD.2006.874581>.
- [24] Tukey JW. Comparing individual means in the analysis of variance. Biometrics 1949;5(2):99–114. <https://doi.org/10.2307/3001913>.